Wear Problems of High-Speed Wheel/Rail Systems: Observations, Causes, and Countermeasures in China

Wanming Zhai
State Key Laboratory of Traction Power,
Southwest Jiaotong University,
Chengdu 610031, China

Xuesong Jin
State Key Laboratory of Traction Power,
Southwest Jiaotong University,
Chengdu 610031, China

Zenfeng Wen
State Key Laboratory of Traction Power,
Southwest Jiaotong University,
Chengdu 610031, China

Xin Zhao[1]
State Key Laboratory of Traction Power,
Southwest Jiaotong University,
Chengdu 610031, China
e-mail: xinzhao@swjtu.edu.cn

Wear problems of wheel/rail systems occurring on the Chinese high-speed railway network in the last decade are summarized and explained together with the corresponding experience of treating them. Focus is placed on uneven wear because even wear is not an urgent issue due to its very low wear rate for the Chinese high-speed railway systems. Two typical problems of longitudinal uneven wear, namely, wheel polygonization and rail corrugation, are introduced in terms of their characteristics, consequences, causes and initiation mechanisms. Next, wheel hollow wear and flange/gauge side wear, as typical problems of lateral uneven wear, are similarly discussed. Validated countermeasures against all these problems are presented at the end of this paper together with further proposals under testing or consideration. This work is principally based on first-hand data collected from field observations, monitoring tests and dynamic measurements, but typical numerical approaches and results are also presented to help explain the observed phenomena. [DOI: 10.1115/1.4048897]

Keywords: High-speed railway, wheel polygonization, rail corrugation, hollow wear, countermeasures

1 Introduction

Since the opening of the first Chinese high-speed line (the Beijing-Tianjin intercity railway) right before the Beijing 2008 Summer Olympics, the high-speed railway has been booming over China. As shown in Fig. 1, the Chinese high-speed railway network had extended to over 35,000 km by the end of 2019, accounting for more than two-thirds of the world total. On an average day in 2018, over 4500 high-speed electrical multiple units (EMUs) ran on the network to transport more than 4×10^6 passengers.

Until the first half of 2017, high-speed EMUs in China could be categorized into 250 km/h and 350 km/h classes corresponding to their top operating speeds (referred to as 250 km/h and 350 km/h EMU hereinafter, respectively). Wheels made of ER8 steel are usually installed on the EMUs with initial diameters of 860 mm or 920 mm (depending on the manufacturer, not on the top speed). Their service lives end as the diameters reach 790 mm or 830 mm (i.e., with allowed wear depths of 35 mm or 45 mm), respectively. The majority of tread profiles are the LMa and S1002CN designs for initial diameters of 860 mm and 920 mm, respectively. High-speed rails are typically made of U71MnG rail steel (approximately equivalent to R260Mn on European tracks) with profiles given by the CN60 design and its derivatives across the whole network. For more information, the reader is referred to related standards, for example, [2–5].

Today, several types of high-speed EMUs and tracks, originating from pioneering countries such as Japan, France, and Germany, are found across the Chinese high-speed railway network (the different wheel diameters and profiles mentioned above are typical examples). This significantly complicates the vehicle-track interactions, especially in the long run. In terms of wheel/rail systems, the experience from the last decade has shown that the present high-speed systems generally meet the requirements of operation at speeds up to 350 km/h when intense monitoring and maintenance of the vehicles and tracks is conducted. For example, wheels and rails are routinely inspected as frequently as every two days to ensure the reliability, availability, and safety of the whole system. Once any excessive damage is found, extra maintenance, supplementing periodic wheel reprofiling (typically every 200,000–300,000 km) and rail grinding (typically every 2–3 years), is scheduled to restore the system to operation in a timely fashion.

The purpose of this review is to summarize the knowledge and experience gained in the context of the Chinese high-speed railway development during the last decade from a series of investigations into the most noticeable wheel and rail wear problems. Some of these wear problems were not found before on other high-speed networks, e.g., high-order polygonal wear of wheels. Extensive first-hand information collected from field observations and monitoring tests is presented in detail, and some

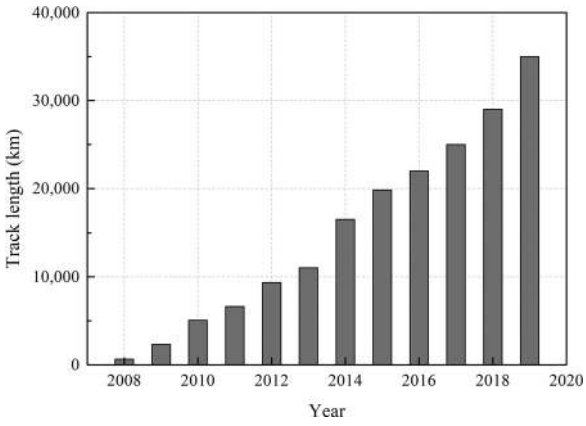

Fig. 1 The rapid extension of Chinese high-speed railway network (data from annual reports of National Bureau of Statistics of China [1])

[1]Corresponding author.

Manuscript received November 18, 2019; final manuscript received October 16, 2020; published online November 11, 2020. Editor: Harry Dankowicz.

countermeasures and their effectiveness are also explained. Since wheel/rail wear is an important engineering problem of applied mechanics, typical numerical models of dynamic vehicle-track or wheel-rail interactions developed for studying wear problems are also introduced together with representative predictions.

2 Even Versus Uneven Wear of Wheel and Rail

A monitoring test found that the natural average wear rate of the wheels on 47 EMUs was 4.5×10^{-6} mm/km at the position of the nominal rolling circle (NRC) [6,7], suggesting that a running distance of 7.78×10^{6} km (approximately 17 years) would be required to reach the wear limit of 35 mm if the artificial wear by reprofiling were ignored. Another set of monitoring tests lasting for 3–7 years on three high-speed lines with design speed of 350 km/h (referred to as 350 km/h lines hereinafter) found that the wear rate of the rail top was 0.05–0.08 mm/year on tangent tracks [8], suggesting a service life of 125–200 years if a wear limit of 10 mm were applied and artificial wear by grinding were ignored. Such low wear rates are attributed to, among others, better driving/braking control implemented in the EMUs and the fact that the minimum radius of curvature is as large as 7000 m for the 350 km/h lines and 3500 m for the 250 km/h lines in China. This implies that wear is not a problem for high-speed wheels and rails if occurring evenly, making frequent and periodic wheel reprofiling and rail grinding affordable.

In contrast, uneven wear, as a result of varied wear levels, has been found to be a significant problem for high-speed wheels and rails. Since wear variations normally result from wheel-rail vibrations excited by irregularities and dynamic wheel–rail interactions are more sensitive to irregularities at a higher speed, uneven wear of high-speed wheels and rails can be considered, to a certain extent, a consequence of system vibrations at high speeds. By its distribution, uneven wear can roughly be classified into two categories, namely, along the longitudinal and lateral directions (corresponding to the circumferential and axial directions for wheels, respectively). In Secs. 3–6, after briefly introducing the research methodology, the most prevalent problems of longitudinal uneven wear, namely, wheel polygonization and rail corrugation, are first explained in detail, followed by those along the lateral direction, namely, wheel hollow wear and wheel flange and rail gauge side wear. The content presented here covers their characteristics, consequences, causes and countermeasures.

3 Methodology

Investigations of uneven wear usually start from reported fatigue or vibration problems such as fracture of rail fastening clips, missing axle box covers of wheelsets, and unacceptable vibrations or noise. To determine their root causes, field observations and measurements are usually conducted first followed, typically, by monitoring and dynamic tests to collect related information. In combination with numerical analyses, the reported problems are often found to be consequences of high frequency vibrations excited by short-wavelength uneven wear on wheels or rails.

Figure 2 summarizes the strategy employed during such investigations. It is seen that focus is placed on collecting empirical data, motivated by the ultimate aim of solving the uneven wear problems in practice. In other words, large amounts of field data help with the understanding of the influences, consequences and development of uneven wear. This also builds a solid basis for further numerical simulations aiming to reveal the initiation mechanism(s) of uneven wear. It is not uncommon that observations, analyses and monitoring tests are conducted repeatedly, so that their relationships may not as unidirectional as suggested in Fig. 2.

3.1 Observations, Measurements and Monitoring Tests. It is well known that almost all dynamic loads sustained by EMUs and tracks are directly caused by or indirectly related to dynamic wheel-rail interaction. Consequently, the observations, measurements, and monitoring tests all focus on the wheel/rail system. Measurements typically focus on wheel/rail profiles (along the lateral direction), surface irregularities or roughness along the longitudinal or circumferential direction, surface hardness, and wheel-rail adhesion, as seen from results shown later. The geometry of uneven wear such as wheel polygonization, rail corrugation and weld irregularities is further derived from the measured longitudinal and lateral profiles, and their development with time is obtained from series of measurements conducted during monitoring tests that usually last longer than a reprofiling or grinding period. Additionally, information about applied wheel reprofiling and rail grinding maintenance is usually recorded during the tests for later use in statistical, correlation, and numerical analyses.

Since vibrations excited by uneven wear may transmit upward into the vehicle system and downward into the track structure, hammer tests of vehicles, tracks and their components in static conditions, and accelerations of vehicle and track components as well as interior noise during running are also measured in some studies. From these dynamic measurements, excitations and transmission of vibrations can be examined in detail. In addition, vehicle/track parameters, different types of resulting damage, running speeds, and so on are also recorded for later analysis.

3.2 Numerical Models. In order to investigate the effects of uneven wear on the wheel–rail interaction and on the dynamic performance of the vehicle–track system, the theory of vehicle–track coupled dynamics [9–11] can suitably be employed for numerical analyses. The rationale of the vehicle–track coupled dynamics theory is to consider the vehicle and the track as one system integrated through the wheel–rail contact. With this theory, the dynamic behavior of the overall 3D vehicle–track system, excited by irregularities such as polygonal wheels and rail corrugation, can be studied comprehensively at low computational costs in the time domain. Figure 3 shows a typical vehicle–track coupled dynamics model [11], to which the polygonal wheels and rail corrugation could be applied as additional irregularities [12–14].

In this model, by analogy with the Hertzian contact theory, the vertical wheel-rail contact force F_N (Unit: N) is calculated by

$$F_N = \left(\frac{1}{G}\delta Z\right)^{3/2} \tag{1}$$

For worn treads, the empirical constant G (m/N$^{2/3}$) is recommended to be [11]

$$G = 3.86 r^{-0.115} \times 10^{-8} \tag{2}$$

where r (m) is the rolling radius of the wheel. Here the time-dependent elastic compression δZ (m) is defined as

$$\delta Z(t) = Z_w(t) - Z_r(t) - Z_0(t) \tag{3}$$

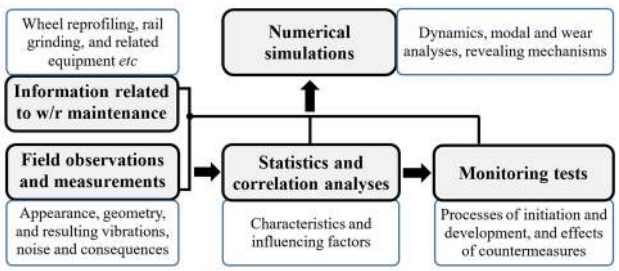

Fig. 2 Typical strategy employed in a study into the uneven wear of high-speed wheel/rail systems in China

where Z_w (m) and Z_r (m) represent the vertical displacements of the wheel and the rail, respectively, and Z_0 (m) the irregularity including the geometry of wheel polygonization or rail corrugation. The tangential wheel-rail rolling contact is simulated with rolling contact theories such as Shen–Hedrick–Elkins theory [15]. Furthermore, wear models can also been implemented into the coupled dynamics model to calculate the resulting wear, see, e.g., Ref. [16].

If detailed contact solutions and the resulting irregular wear are also of interest, a transient wheel–rail rolling contact finite element (FE) model [17–21], for example, the one in Fig. 4, can be employed. In such a model, the actual wheelset and rail geometry are meshed by solid elements with a minimum size of 1.0 mm, typically resulting in millions of nodes, in order to solve the normal and tangential contact using a surface-to-surface contact algorithm developed based on the penalty method. An explicit

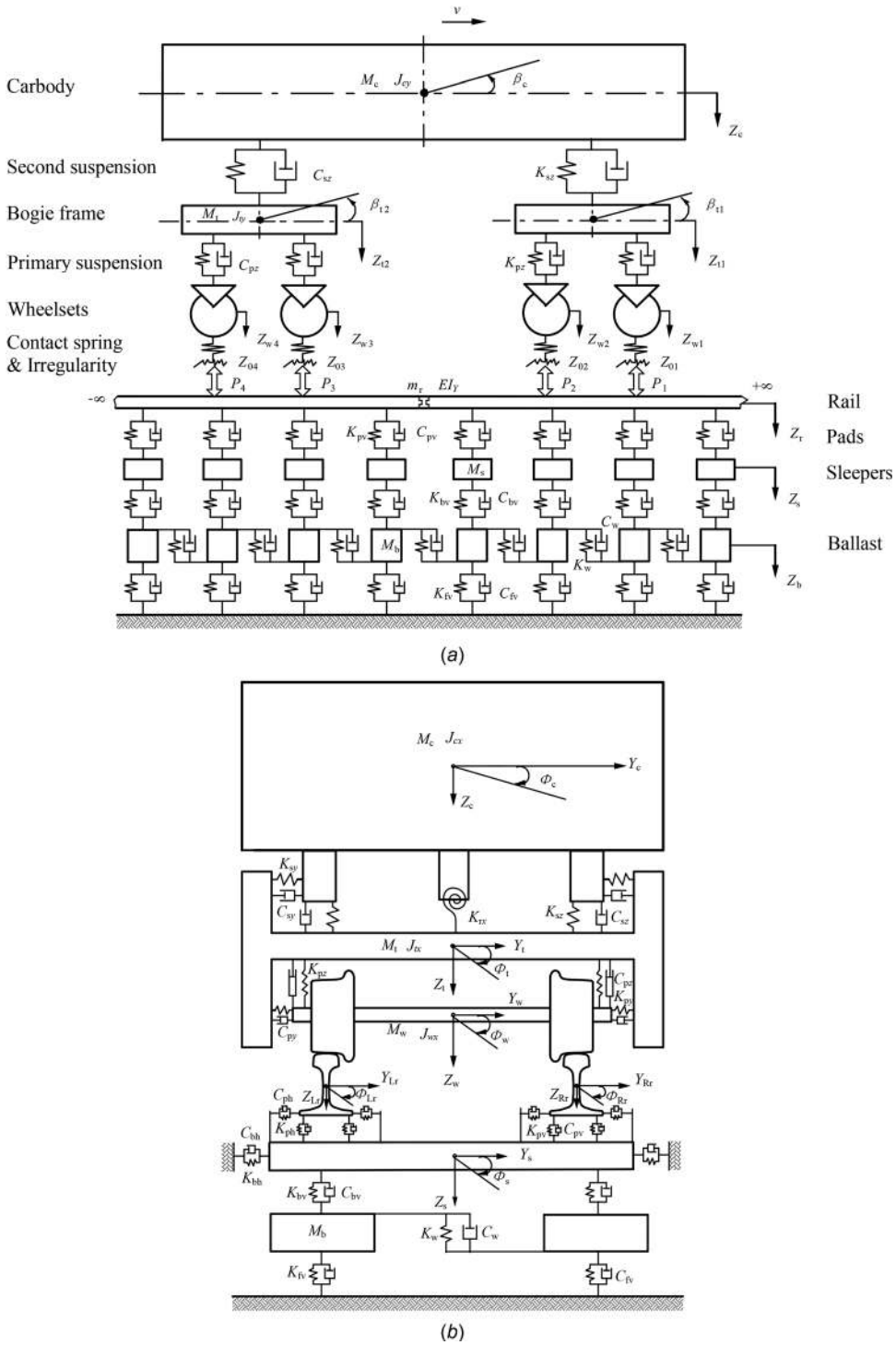

Fig. 3 A typical vehicle-track coupled dynamics model, (*a*) side view and (*b*) end view [11]. A ballasted track is illustrated as an example. *M, J, β, Φ, K, C* and *P* are mass (kg), moment of inertia (kg·m^2), pitch angle (rad), roll angle (rad), stiffness (N/m), damping (N·s/m) and vertical contact force (N), respectively. m_r and EI_r are the mass per meter (kg/m) and bending stiffness (N·m^2) of rail, respectively.

time-integration scheme is further implemented, leading to a very short time-step (10^{-8} ~10^{-7} s) due to the conditional stability of explicit schemes. Thus, such a model is suitable for analyses of high frequency dynamics in the time domain, but at a high computational cost.

Wheel-rail rolling-sliding and the corresponding creepage are simulated by setting different translational and rotational speeds of the wheelset, and applying the corresponding time-dependent drive/braking torque $T(t)$. The longitudinal creepage ξ (dimensionless) is defined by

$$\xi = \frac{\omega r - v}{(\omega r + v)/2} \tag{4}$$

where v (m/s) and ω (rad/s) are the translational and angular speeds of the wheelset, respectively. The time-dependent torque $T(t)$ (N·m), determined by the acceleration $a(t)$ (m/s^2) and the related angular acceleration $\dot{\omega}(t)$ (rad/s^2) of the wheelset, is given by

$$T(t) = F_\tau(t) r(t) + J_w \dot{\omega}(t) \tag{5}$$

$$a(t) = F_\tau(t)/M_T \tag{6}$$

where, $F\tau$, M_T (kg), and J_w (kg·m^2) are the tangential contact force (or creep force) transmitted between the wheel and the rail, mass of the whole vehicle system considered in the model, and the moment of inertia of the wheel around the symmetry axis, respectively. The wheel radius r (m) varies with time in the presence of wheel irregularities. In the case of steady-state rolling with unsaturated friction, the acceleration and the angular acceleration is related by

$$\dot{\omega}(t) = a(t)/r(t) \tag{7}$$

In addition, the primary suspension of the vehicle, the discrete support of the rails and so on can all be taken into account properly in the transient FE model, so that the high frequency structural vibrations of the vehicle–track system are simulated accurately together with the continuum vibrations of the wheelset and the rails. Irregularities such as wheel polygonization and rail corrugation are considered by modifying the surface geometry of the wheel and rail. Till now, transient rolling-sliding at speeds up to 500 km/h has been treated using this model. Very recently, wear models have been implemented into the transient FE model to calculate the transient irregular wear in 3D based on the detailed contact solutions [21], providing an appealing tool for studies into uneven wear.

To identify the eigenmodes resulting in or excited by the uneven wear, modal analyses have also been conducted using methods like FE, and the obtained eigenfrequencies have been compared with those measured in hammer and dynamic tests [22–25]. Such analyses could provide important information for better understanding of the problems of uneven wear and their consequences. For clarity, the three main types of numerical models mentioned above and their functions are summarized and illustrated in Fig. 5.

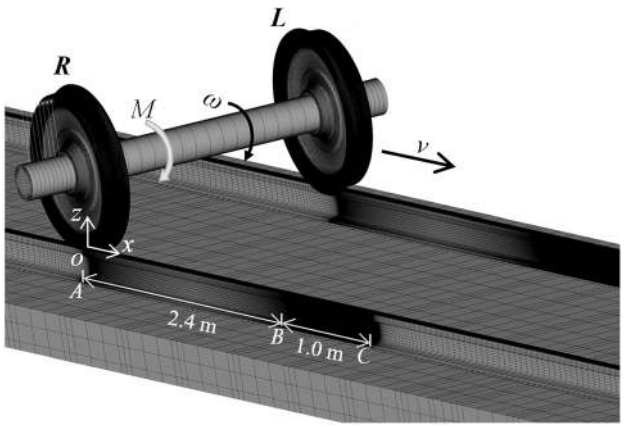

Fig. 4 A transient high–speed wheel–rail rolling contact FE model [21] developed to calculate the detailed contact dynamics under high frequency excitations. Both time-dependent force excitations and short-wavelength irregularities such as high-order wheel polygonization can be applied.

4 Uneven Wear Along the Longitudinal Direction

Uneven wear along the longitudinal direction can occur both locally and continuously, being composed of one or two wavelengths or lasting for many continuous wavelengths. Although local uneven wear such as wheel flats and irregular rail welds also exist in high-speed wheel/rail systems, their further study is not urgent because of the following facts: (1) their causes are well known: wheel flats are mostly related to low adhesion and braking systems/strategies [26,27], and irregular welds are caused by material inhomogeneity resulting from the welding process [28]; (2) their consequences are acceptably managed with countermeasures developed in the past. In contrast, in the last decade, continuous uneven wear was found to result in unacceptable consequences, spurring on great research efforts, as will be seen in the following. Note that material detachments resulting from rolling contact fatigue (RCF) such as spalling and shelling, which were occasionally observed on a few EMUs [7], are not counted as uneven wear in this paper.

4.1 Wheel Polygonization. Wheel polygonization describes periodic deviations of the radius (i.e., out-of-roundness) resulting from uneven wear along the circumference. The number of periods or, equivalently, the wave number contained around the circumference is usually defined as the order (n), as illustrated in Fig. 6. Obviously, the excitation frequency of a polygonal wheel f_n (Hz) influencing the wheel-rail dynamics is determined by the order of the polygonization, the wheel radius r (m) and the rolling speed v (m/s)

$$f_n = \frac{v}{\lambda_n} = \frac{vn}{2\pi r} \quad n = 1, 2, 3\ldots \tag{8}$$

where, λ_n (m) is the corresponding wavelength. Note that several orders usually coexist in practice, further complicating the wheel-rail interaction, and their amplitudes and influences can be separated from each other using techniques such as Fourier analysis.

4.1.1 Studies in Early Days. Nielsen and Johansson [27,29] studied wheel polygonization occurring on ICE trains and drew the following conclusions: the polygonization was usually dominated by 1st- to 5th-order (i.e., low orders) with amplitudes of up to 1 mm, and was only found on disk-braked wheels; 3rd-order

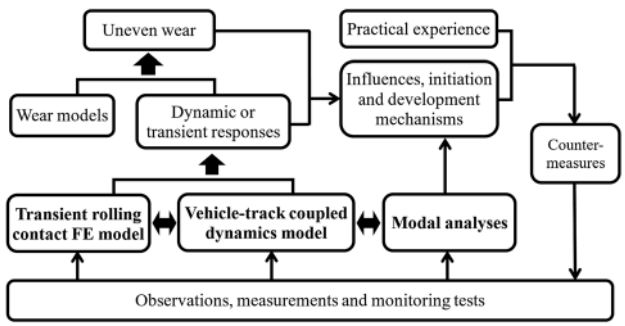

Fig. 5 Three main types of numerical models employed in studies of uneven wear

polygonization was common for solid wheels while second-order polygonization occurred for rubber sprung wheels; an initial and slight 3rd-order polygonization usually resulted from the fixation of the wheels during machining by claw clamping in a three-jaw chuck (the three radius minima corresponded to the clamping positions), and was amplified during running, eventually leading to substantial 3rd-order polygonization; other possible initiation mechanisms included inhomogeneous material around the circumference and coupling to the eigenmodes of wheelsets. Morys [30] combined a multibody model and a wear model to study the exacerbation of existing low-order polygonization for an ICE-1 carriage, and found that its development was dominated by the bending eigenmodes of the wheelset (typically 50–80 Hz). Meinke and Meinke [31] believed that the imbalance of wheelsets, especially dynamic imbalance, was the root cause of low-order wheel polygonization. Deuce [32] surmised that wheels with low-order polygonization might result from a system interaction issue or by a wheel machining issue, while higher orders (>5th, according to the authors' understanding of the context) might be observed on resilient wheels.

On many Stockholm subway trains, 3rd-order polygonization with peak-to-peak amplitudes up to 1.2 mm were observed, and Johansson and Andersson [33,34] argued that they were also caused by initial irregularities left by the fixation of the wheels during machining. Recently, Jin et al. [35] observed 9th-order polygonization on disk-braked wheels on a type of metro trains equipped with linear induction motors, and determined its cause to be the first bending resonance of the wheelset. Such an initiation mechanism was later confirmed by the application of a newly designed wheelset (a thicker axle was used to shift the frequency of the related eigenmode) [36].

For block-braked wheels, another type of polygonization with short wavelengths of 30–80 mm was observed in the Netherlands and other countries [37]. Since the wavelength is similar to short pitch rail corrugation, it is also referred to as wheel corrugation. Its cause was found to be hot spots resulting from thermoelastic instability of the block-tread contact, i.e., more material was worn away on hot spots where larger expansion occurred, and the amplitude was usually smaller than 10 μm [29,37,38]. Johansson [34] further found that the roughness level in the wavelength range of 30–80 mm was increased because of tread braking, even if no wheel corrugation was reported.

It has been widely recognized that polygonal wheels can significantly affect the wheel–rail interaction, resulting in larger contact forces and higher levels of vibrations and noise, further lowering the riding comfort and accelerating the damage of related components. To study these consequences and the development of polygonization, numerical models have been developed to calculate the dynamic vehicle-track interaction in the presence of wheel polygonization (long-wavelength irregularities), e.g., Refs. [39] and [40]. According to Ahlbeck and Harrison [40], the vibrations resulting from long-wavelength irregularities are of relatively low frequencies, so that they can transmit more energy to axle bearings and vehicle components, leading to severe damage there. The same also occurs on the track side, resulting in damage on components like fastening clips. Note that about 20 years ago, numerical analyses of wheel polygonization were quite uncommon compared to those of wheel flats and rail corrugation [29].

4.1.2 *Observations and Measurements*

4.1.2.1 A typical case. In 2014, a running test of a newly designed 250 km/h EMU was conducted under full loading on a new high-speed track in south China (referred to as line 1 hereinafter; about 270 km long). At that time, line 1 had not yet been put into commercial operation, so that the test EMU ran at an almost constant speed of 250 km/h without stops between the terminal stations (two round trips each day). After running slightly more than 70,000 km, the test was suspended because of loose bolts and missing axle box covers (see Fig. 18 below). Careful subsequent examinations showed that fierce vibrations resulting from high-order wheel polygonization were the causes.

Figure 7(*a*) shows the out-of-roundness of the wheels measured in 2014 (after the test suspension). An upper limit curve for the acoustic rail roughness level proposed in ISO3095 is plotted in red (and similarly in some later figures; such a limit is absent for high-speed wheel roughness) for comparison and reference. It is first seen that the measured roughness peaks are significantly higher than the ISO3095 line at around 14th- and 23rd-order, suggesting that 14th- and 23rd-order polygonization is present. Furthermore, the amplitude of the 23rd-order was larger than 20 dB (defined with respect to 1 μm; 20 dB corresponds to peak-to-peak amplitude of 0.02 mm) for many wheels with a maximum of 34 dB (corresponding to peak-to-peak amplitude of 0.1 mm), while the 14th-order exceeded the same levels on many fewer wheels. This indicates the dominant role of the 23rd-order polygonization in the out-of-roundness of the wheels. Note that the out-of-roundness data shown in this paper were all measured at NRC. No considerable difference was found between the trailing and the powered wheelsets, but a significant phase difference did exist between the polygonization on the two wheels of a wheelset (thorough studies of this phase difference is still lacking).

In the winter of 2014, the running test was continued on the same line and under identical running conditions, before which all wheels of the EMU were reprofiled on turning lathes (hereinafter referred to as the first reprofiling) to restore their roundness and profiles. The effectiveness of the polygonization removal was confirmed through roundness measurements after the reprofiling; see Fig. 7(*b*) for an example, in which the roundness of the same wheel after the reprofiling is compared to that before. In the beginning of 2015 or after running 34,000 km, the EMU was moved to another line in north China (line 2; about 350 km long and in commercial operation for about three years) and the test was continued at an almost constant speed around 200 km/h.

From the measurements shown in Fig. 8(*a*) it is seen that the high-order polygonization reoccurred and that the amplitude increased with the running distance as expected when continuing running at 250 km/h on line 1, but stabilized or stopped growing unexpectedly when running at 200 km/h on line 2 (see Fig. 8(*b*)).

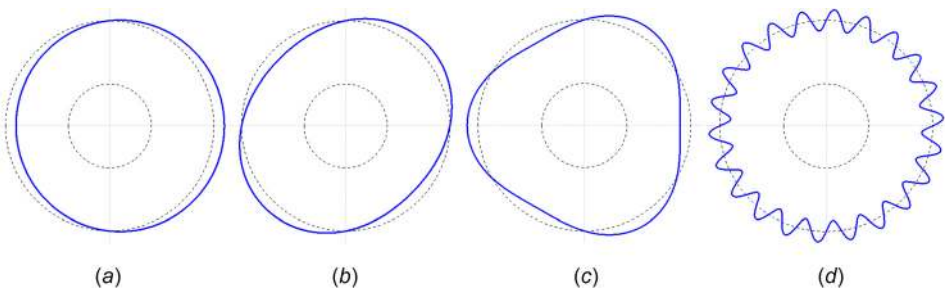

Fig. 6 Schematic diagrams in a polar coordinate system of wheels, each having one order of polygonization: (*a*) 1st-order (eccentricity), (*b*) 2nd-order (ellipse), (*c*) 3rd-order, and (*d*) 22nd-order

Consequently, for all wheels, the amplitude of the 23rd polygonization was much lower at 64,000 km after the first reprofiling than after about 70,000 km in the original test shown in Fig. 7, and even below the ISO3095 line for some wheels (see Fig. 8(*b*) for an example). Thus, the track and the running speed seem to be important factors influencing the occurrence of high-order polygonization.

Reassured by the stabilized polygonization, the EMU was taken to another high-speed line in north China (line 3) for commercial operation at 71,000 km after the first reprofiling or at the end of 2015, and all wheels were reprofiled for a second time before running. Since the average interval between stations on this line is about 20 km, the EMU had to accelerate, decelerate, and stop frequently and the maximum speed of 250 km/h could only be reached in some particular sections (e.g., some long tangent sections). Obviously, such a running condition is very different from the constant running speeds on lines 1 and 2.

Monitoring tests in 2016 surprisingly showed that no high-order polygonization occurred up to a running distance of 127,000 km after the second reprofiling, and that the roughness level was almost completely below the ISO3095 line, as shown in Fig. 8(*c*). In other words, the high-order polygonization occurring in the previous tests did not appear during the commercial running on line 3, even though no changes were made to the EMU except for wheel reprofiling. Possible reasons behind these phenomena will be explained in detail later with more test results. Note that low-order polygonization, which was also recognizable on high-speed wheels, e.g., the 1st-order polygonization in Figs. 7(*a*) and 8, is not explained further in this paper because it does not result in significant consequences (probably due to its low passing frequency).

4.1.2.2 Polygonization observed earlier and their origins. As early as 2011, wheel polygonization was found on the wheels of some 350 km/h EMUs in China. Figure 9 shows the development of the out-of-roundness on a wheel during monitoring tests in 2011 and 2012. The figures show that first-, sixth-, eighth-, 12th-, and 20th-order polygonizations co-existed with none of them dominating the out-of-roundness, in contrast to the data in Fig. 7. Further, the polygonization gradually grew in amplitude with the running distance, as seen from the measurements at 150,000 and 270,000 km, while the patterns remained quite similar. At 300,000 km the wheels of the EMU were reprofiled for the first time, after which very similar out-of-roundness re-occurred at the running distance of 400,000 km or 100,000 km after the reprofiling (see Fig. 9).

It should be noted that Fig. 9 shows a worst case scenario observed during the monitoring test, and that most of the monitored wheels (of four 350 km/h EMUs) were much better in terms of roundness. No significant consequences had been reported at that time [43]. Careful examinations showed that the polygonization components on most wheels were of relatively low orders, and two main origins were isolated. First, the 1st- and 3rd-order polygonization, which was found on many new wheels, was understood to originate from the production process of wheels. The 3rd-order was attributed to the fixation of wheels during machining, as mentioned in Sec. 4.1.1. Second, polygonization of the 4th- to 6th-order and 10th- to 13rd-order was caused by the noncircular drive disks on turning lathes, as confirmed by measurements of newly reprofiled wheels and those after small running distances. Figure 10(*a*) shows the measurement of a newly reprofiled wheel of a 350 km/h EMU, in which polygonization of 4th- to 6th-order, 10th- to 13th-order and 18th-order was recognizable (note that their amplitudes were far below the ISO3095 line). The concrete order of such polygonization is determined by the diameter ratio and the slip between the railway wheel and the drive disks, i.e., an eccentric drive disk (1st-order polygonization) may lead to 4th- to 6th-order polygonization on the newly reprofiled wheels, as indicated in Fig. 10(*b*), and higher orders are expected if the two drive disks are both eccentric and contacting the wheel with different phase angles.

A series of measurements carried out in 2011 and 2012 showed that many drive disks were indeed eccentric on many lathes in China. Since then, the railway industry has gradually learned to maintain the drive disks in order to avoid the polygonization caused by reprofiling. Today, polygonization of relatively low orders is well under control, whereas polygonization of high orders (larger than about 12) has become a serious threat to the stability and safety of high-speed EMUs, as presented in Sec. 4.1.2.1 and further explained below.

4.1.2.3 Typical high-order polygonization. A large number of measurements have shown that high-order polygonizations are typically of 18th- to 23rd-order. The reasons for such range of orders are threefold: (1) the diameters of wheels continuously decrease due to wheel/rail wear and reprofiling, leading to a lower polygonization order for a fixed wavelength, see Fig. 11 for examples; (2) the eigenfrequency corresponding to polygonization changes with the EMU type, resulting in different wavelengths and further different orders under the same speed and wheel diameter (for example, the wavelength is about 160 mm for the EMU in Fig. 11, but 145 mm for that in Fig. 12); (3) the fixed

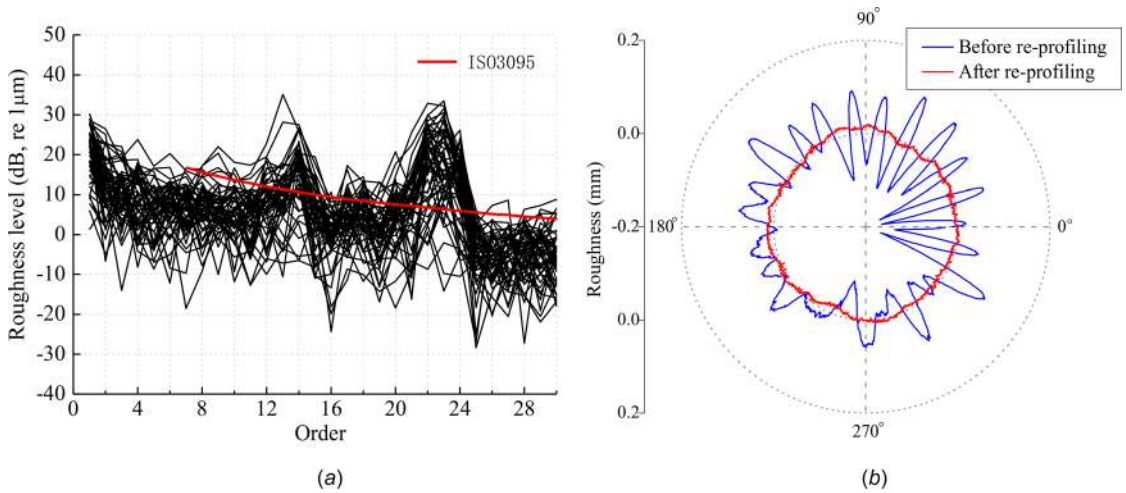

Fig. 7 Out-of-roundness of wheels (Φ860 mm) on the test 250 km/h EMU: (*a*) roughness spectra of all 64 wheels before the first reprofiling (every curve corresponds to one wheel) [41], and (*b*) comparison of the roundness of a wheel before and after the first reprofiling [24]. The range of the ordinate axis is set to be −0.2 to 0.2 mm in (*b*) to clearly show the radius variation caused by polygonization.

eigenfrequency results in varying wavelength and polygonization order as the speed changes. Figure 12 shows the polygonization orders observed during a specially designed on-line test carried out on a commercial line in 2017, for which a 350 km/h EMU equipped with wheels of different diameters was used to run at an almost constant speed of 300 km/h. Such results confirmed that the wavelength of the occurring polygonization was indeed approximately fixed and the resulting order increased with the diameter. As a supplement, Fig. 13 shows additional examples of measured high-order polygonization in a polar coordinate system.

4.1.2.4 Irregular plastic deformation on polygonal wheels. Although high-order polygonization is a consequence of irregular wear, the out-of-roundness and the resulting dynamic forces can also lead to irregular plastic deformation on the wheel surface. This can be seen from Fig. 14, in which the surface hardness variation measured at NRC follows the measured geometry variation of the high-order polygonization. Observations during wheel reprofiling showed that a radial cut of 0.5–1.0 mm, which was the typical range applied early on, could not remove the unevenly hardened layer completely. To avoid the easy reoccurrence of polygonization from remaining hardness deviations, a radial cut above 2 mm is currently adopted for reprofiling of polygonal wheels.

4.1.3 Influences and Consequences

4.1.3.1 Significant wheel–rail interactions. With a high–speed vehicle–track coupled dynamics model specially developed for the EMU in Figs. 7 and 8, the vertical dynamic wheel-rail contact forces were calculated in the presence of measured polygonization in Ref. [13]. From the calculated results shown in Fig. 15 it is seen that the peak forces caused by the wheel out-of-roundness shown in Fig. 7(*b*) are up to 157.0 kN, and decrease after reprofiling (polygonization removed) to 82.5 kN (the static wheel load 70.6 kN). Contact loss (i.e., the contact force vanishes or wheel and rail separate from each other) is expected at some instants when the polygonization is present. Based on a series of coupled dynamics analyses, Chen et al. [45] concluded that the influence of high-order polygonization was insignificant on safety and stability of running vehicles. Chen et al. [14] found that high-order polygonization did not affect the dynamic performance of the subgrade as severely as low-order ones. More studies on the wheel–rail interactions at high-order polygonization can be found in Refs. [25] and [46–49], where similar coupled dynamics models were employed.

Evidence of significant dynamic interactions caused by polygonal wheels has also been found in the record of axle box accelerations and noise. For example, the development of 18th-order polygonization occurring on an EMU wheel running at a maximum of 300 km/h resulted in a significant increase of the vertical axle box acceleration at its passing frequency of about 580 Hz, from an amplitude of about 0.5 g right after reprofiling to 14.3 g at 170,000 km, as shown in Fig. 16. From the interior noise measurements of another 350 km/h EMU shown in Fig. 17, it is seen that the noise was much louder when polygonal wheels were present than that absent. These suggest that the vibrations excited by

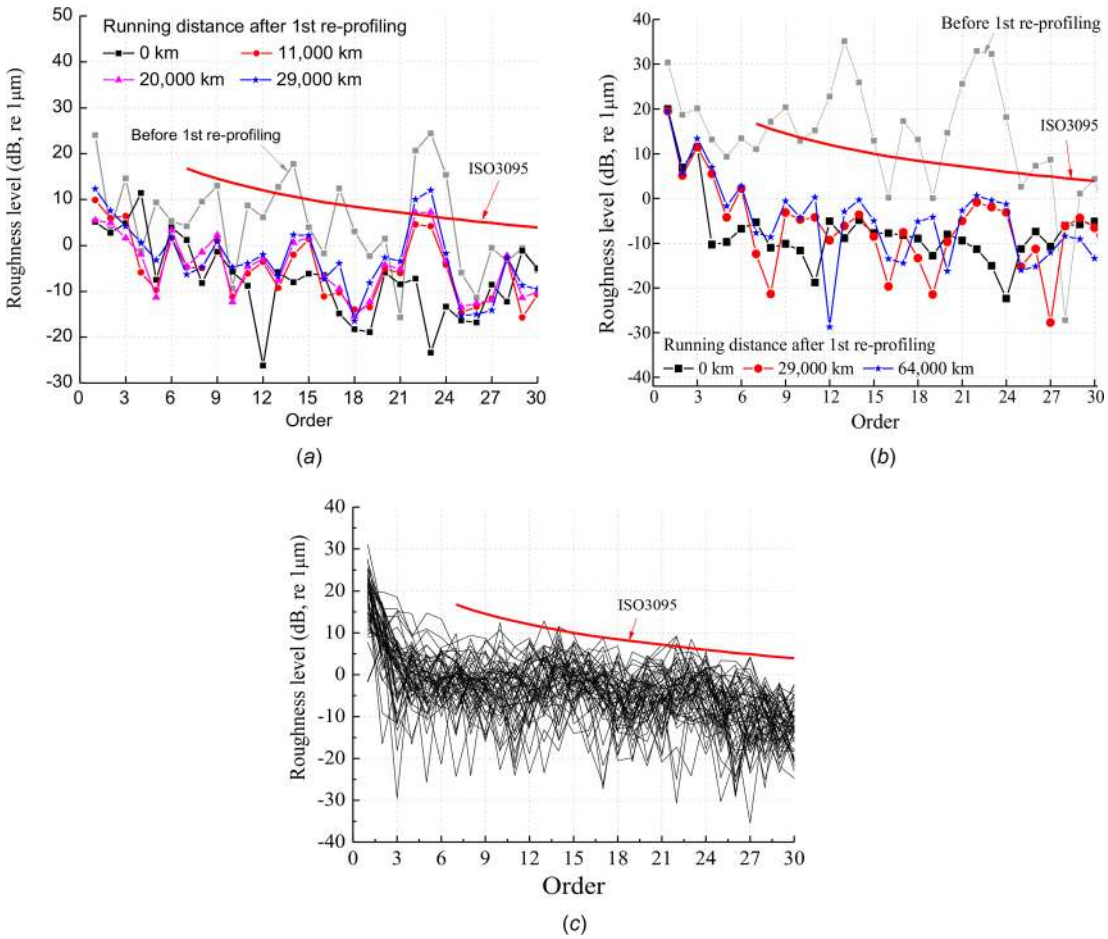

Fig. 8 Out-of-roundness of the wheels (Φ860 mm) on the test 250 km/h EMU measured in 2014–2016 [24,41]. Roughness spectra of (*a*) a wheel during continuous running at an almost constant speed of 250 km/h on line 1, (*b*) another wheel during continuous running at almost constant speeds of 250 and 200 km/h on lines 1 and 2, respectively, and (*c*) all wheels after commercial running over a total distance of 127,000 km at varying speeds on line 3.

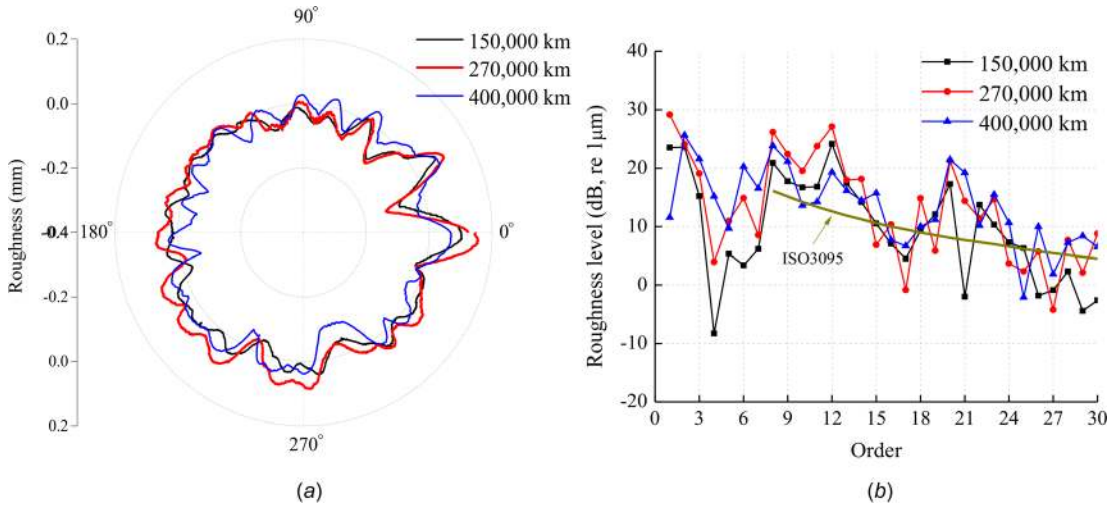

Fig. 9 Development of polygonization on a wheel (Φ920 mm) of a 350 km/h EMU running on Beijing-Shanghai high-speed line [42]. Measurements were carried out in July 2011, March 2012, and September 2012, respectively. The maximum speed was 350 km/h before July 2011 and 300 km/h thereafter. The wheel was reprofiled at the running distance of 300,000 km. (*a*) In a polar coordinate system, and (*b*) roughness spectra.

high-order polygonization could transmit to the car body (confirmed by more measurements), resulting in larger accelerations and noise emissions there. In a word, high-order polygonization would greatly reduce the ride comfort of high-speed EMUs.

4.1.3.2 Dynamic fatigue damage. Due to upward and downward transmissions of the additional vibrations caused by high-order polygonization, some key components and accessories, e.g., of the bogies and the fastenings, may vibrate severely during running. Under certain extreme conditions, this might lead to dynamic fatigue damage such as those in Fig. 18. This was actually the direct impetus for intensive investigations on polygonization of high-speed wheels in the past years in China.

4.1.4 Root Causes and an Initiation Mechanism. A series of on-board and track side dynamic measurements have been conducted in the past years together with necessary numerical simulations to isolate the root causes of high-order polygonization. This section takes the 23rd-order polygonization occurring on the 250 km/h EMU mentioned in Sec. 4.1.2.1 as an example to reveal the typical results obtained, based on which the root causes are identified and an initiation mechanism is further proposed.

4.1.4.1 Related eigenmodes and root causes. From the wavelength of the polygonization it is easy to find that its passing frequency is 591.0 Hz at 250 km/h. Results of a hammer test on a bogie (in static conditions) showed that there were indeed some significant vibration peaks around the passing frequency, as shown in Fig. 19(*a*). This is even more obvious in the running test results in Fig. 19(*b*) where newly reprofiled wheels (without polygonization) were installed for measurements. Furthermore, Fig. 19(*b*) shows that the polygonization-related vibration could effectively transmit from the wheelset to the bogie frame, which explains well the influences and consequences shown in

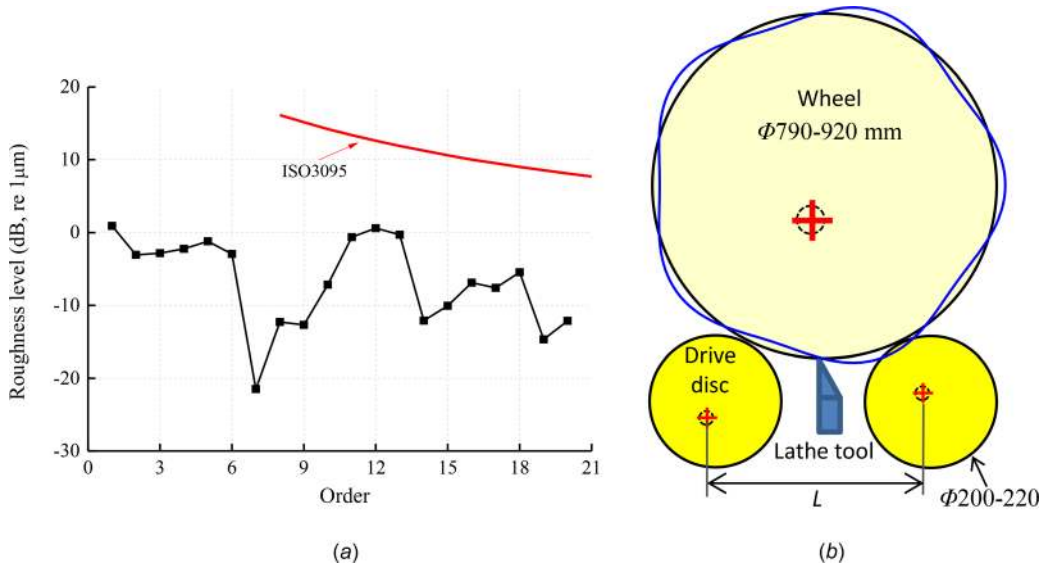

Fig. 10 Polygonization resulting from the reprofiling process on a typical turning lathe used in China [43,44]. (*a*) The roughness spectrum of a newly reprofiled wheel of a 350 km/h EMU in 2011. (*b*) A schematic diagram of the lathe, in which the out-of-roundness of the drive disks (with eccentricity) is indicated by exaggerated positions of their centers.

Figs. 16–18. The essence behind these phenomena is that significant eigenmodes of the bogie and its main components exist around the passing frequency, as shown in Fig. 20.

In contrast, no track eigenfrequencies and eigenmodes were found around the passing frequency under either static or running conditions, as shown in Fig. 21. Hence, the high-order polygonization tends to be a consequence of certain excited eigenmodes of vehicles, most probably of bogies or wheelsets. Note that the pinned-pinned resonance of the track (at 1015 Hz) is very clear in Fig. 21(*a*), and the peak at 750 Hz in Fig. 21(*b*) is due to rail corrugation with a wavelength of 60–80 mm (further discussed below in Sec. 4.2.2.2)).

4.1.4.2 A proposed initiation mechanism. The eigenmodes presented above should exist for any bogies, even though the corresponding frequencies probably vary with the detailed design. However, high-order polygonization does not occur on every wheel in reality. To the authors' best understanding, high-order polygonization can only come into being when the following prerequisites are met: (1) the eigenmode is excited effectively; (2) the wavelength of the resulting uneven wear divides the circumference of the wheel (without a remainder). If only the first is met, polygonization can hardly occur because the resulting contact force oscillations and wear pattern do not repeat themselves in every cycle, but are constantly modified in each cycle instead, as indicated in Fig. 22.

Considering that the wavelength is determined by the speed and the eigenfrequency, it can be expected that the occurrence of high-order polygonization should be quicker or easier when the EMU runs at certain specific speeds (the corresponding wavelengths divide the wheel circumference), especially when the speeds last for long time. Furthermore, high-order polygonization is probably dependent on the design of track lines with different speeds and distributions of stations (the speed varies greatly when entering and leaving stations). Actually, these phenomena have been observed in the field, as presented in Sec. 4.1.2.1. In addition, the diameter of a wheel constantly decreases due to wear and reprofiling during its service life, so that polygonization should occur more easily at certain stages when the circumference is divided by the wavelengths, and the order of polygonization should decrease gradually with the running distance, as confirmed by the measurements in Figs. 11 and 12.

4.1.5 A Short Summary. Characteristics of the most detrimental polygonization on high-speed wheels in China are summarized as follows.

(1) Of high orders (larger than about 12) and high frequencies. Taking the 23rd-order polygonization shown in Sec. 4.1.2.1 as an example, its wavelength is 117.5 mm for a new wheel (Φ860 mm), corresponding to a passing frequency of 591.0 Hz at 250 km/h.
(2) Wheel diameter dependent. The order of polygonization decreases gradually as the diameter reduces due to wear and reprofiling.
(3) Occur more easily when running at constant speeds.
(4) Lead to fiercer vibrations, larger contact forces, louder noise, and further accelerated dynamic fatigue damage of some vehicle and track components.
(5) Should be a consequence of excited vehicle eigenmodes, and tend to occur when the wavelengths divide the wheel circumference.

Note that the wavelength of such high-order polygonization is much shorter than those on the ICE trains [27,29,32,33], but significantly longer than those of the wheel corrugation reported in Refs. [29] and [33]. At present, arguments still exist about the

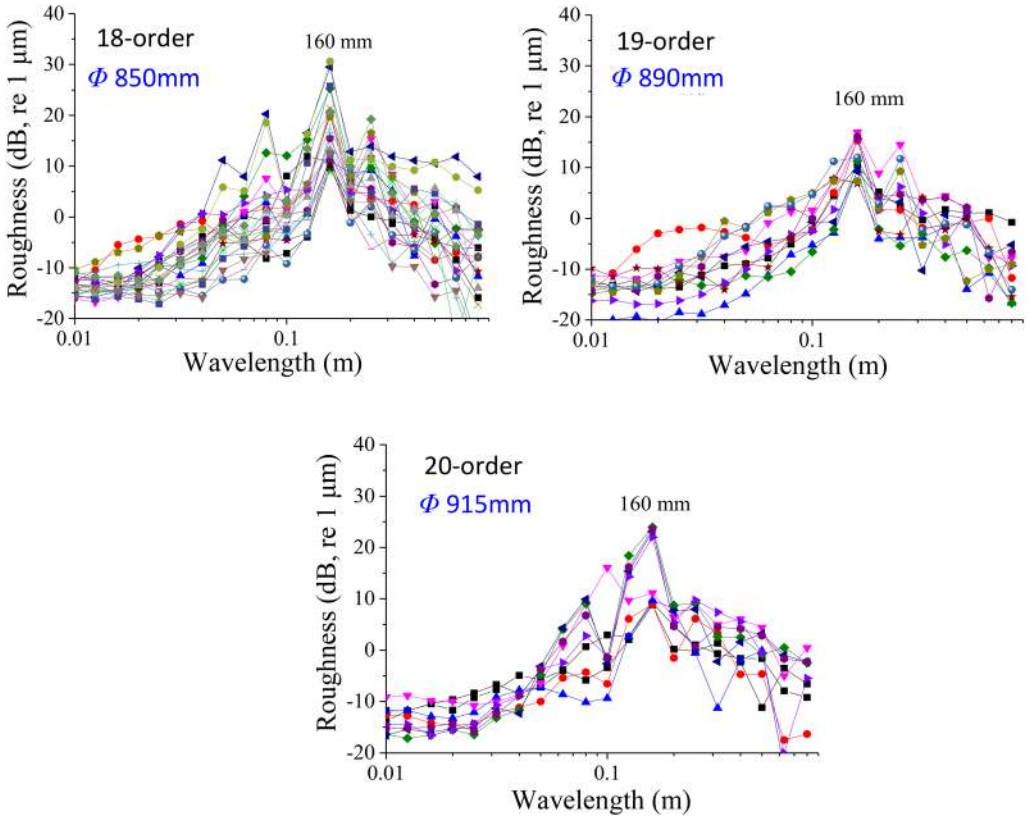

Fig. 11 Reduction of the polygonization order as the wheel diameter decreases, observed on a 350 km/h EMU running at speeds up to 300 km/h in 2015 and 2016. Each curve represents one wheel, and the wavelength is about 160 mm.

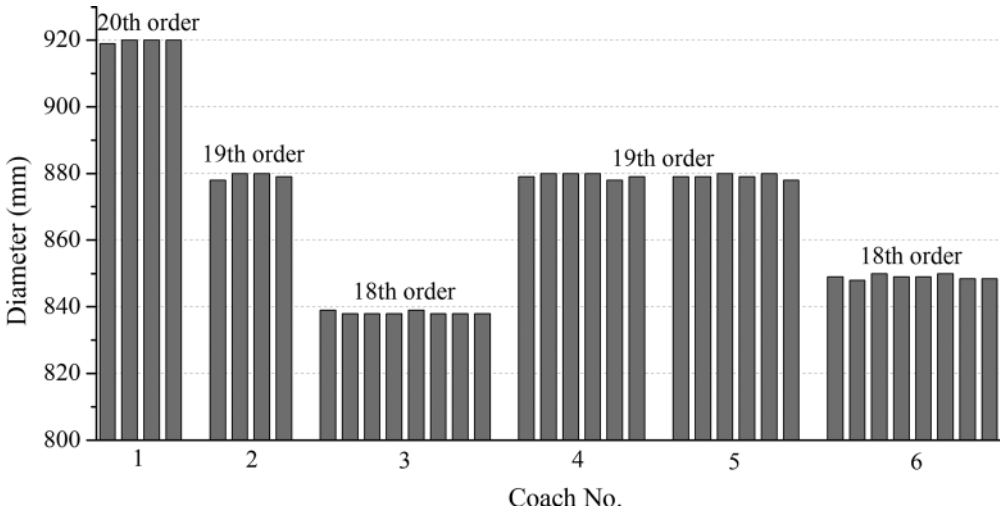

Fig. 12 Polygonization orders observed during a specially designed test carried out on a commercial line in 2017 using a 350 km/h EMU equipped with wheels of different diameters and running at 300 km/h. Every column corresponds to one wheel infected by the high-order polygonization with the wavelength of about 145 mm. This test was specially arranged by China Railway.

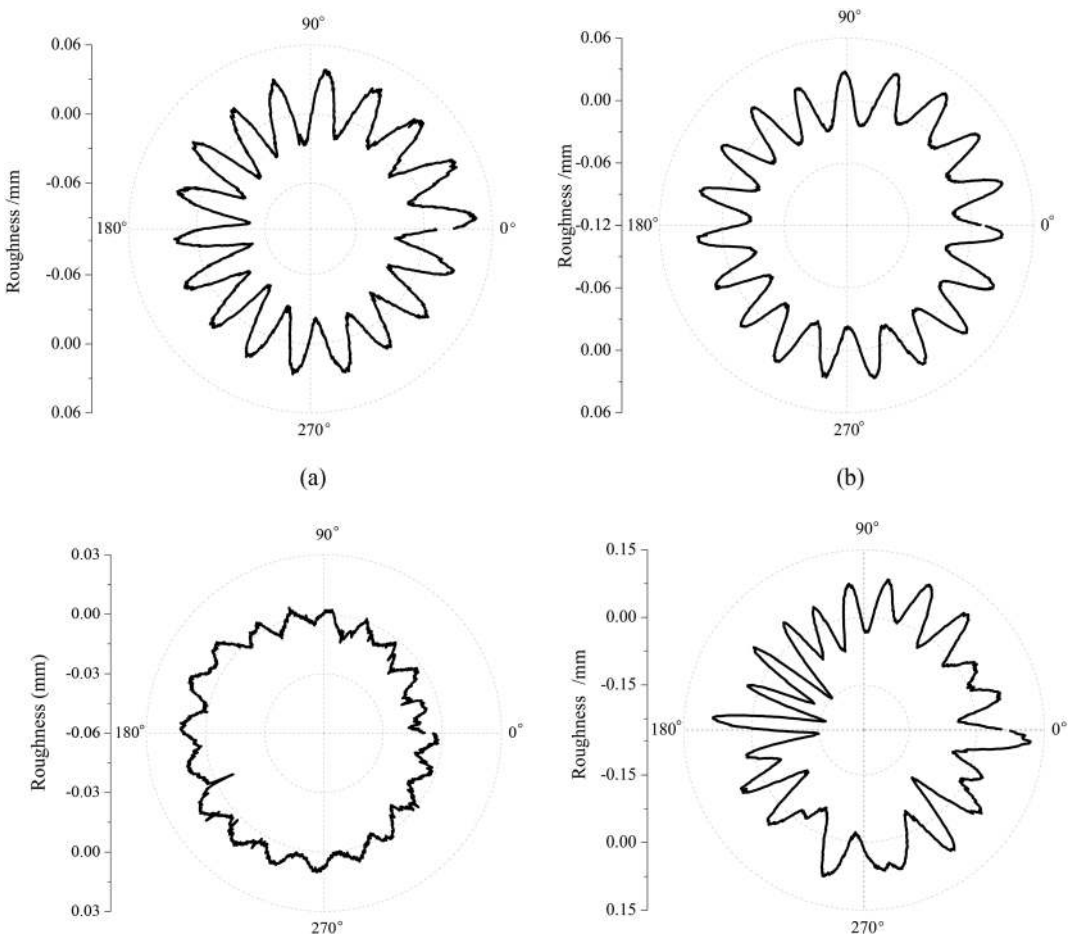

Fig. 13 Additional examples of high-order polygonization occuring on wheels of Chinese high-speed EMUs in 2014–2016. (*a*) 18th-order, running at 300 km/h, (*b*) 19th-order, running at 300 km/h, (*c*) 20th-order, running at 300 km/h, and (*d*) 22th-order, running at 250 km/h.

initiation mechanism of high-order polygonization, e.g., a different opinion was reported in Ref. [50]. Low-order polygonization like those on the ICE [27,29] and metro [35] trains have also been observed on high-speed wheels, but have not been found to result in significant consequences. For more information about wheel polygonization, especially of that occurring on metro vehicles and locomotives, the reader is referred to another recently published review [51].

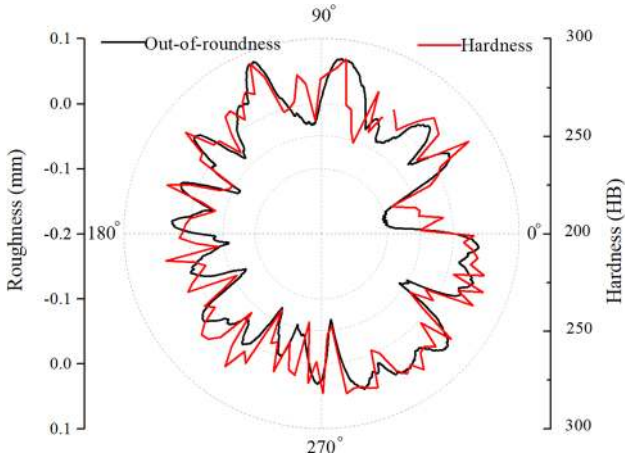

Fig. 14 Out-of-roundness and surface hardness around a wheel of the 350 km/h EMU in Fig. 9. Measured in March 2012 [43].

4.2 Rail Corrugation. Recognized for over a century as a significant problem, rail corrugation has been studied intensively and continuously. Many excellent review articles on rail corrugation have been published in the literature [52–57]. Thus, this section will just focus on the specific corrugation problem occurring on Chinese high-speed rails.

4.2.1 Observations and Measurements. In 2011, short pitch rail corrugation (referred to simply as corrugation hereinafter) was first observed on a newly opened Chinese high-speed line (a 350 km/h line) just after two months of commercial running, causing great concern in the industry [20]. Field observations showed that the corrugation occurred on both tangent tracks and curves of the main line. Roughness measurements by a corrugation analysis trolley showed that the corrugation depth was up to 0.15 mm (peak-to-peak amplitude), and two corrugation components $C1$ and $C2$ were found in every corrugated section with wavelengths of 60–80 mm and 120–160 mm, respectively. Hammer tests and FE simulations showed that $C1$ could be a consequence of the vertical pinned-pinned resonance of the track, while $C2$ appears to be a consequence of a vertical bending mode of the rails [22]. At some locations, $C1$ dominated the roughness of corrugation, while $C2$ was the dominant source of roughness at others, as can be seen

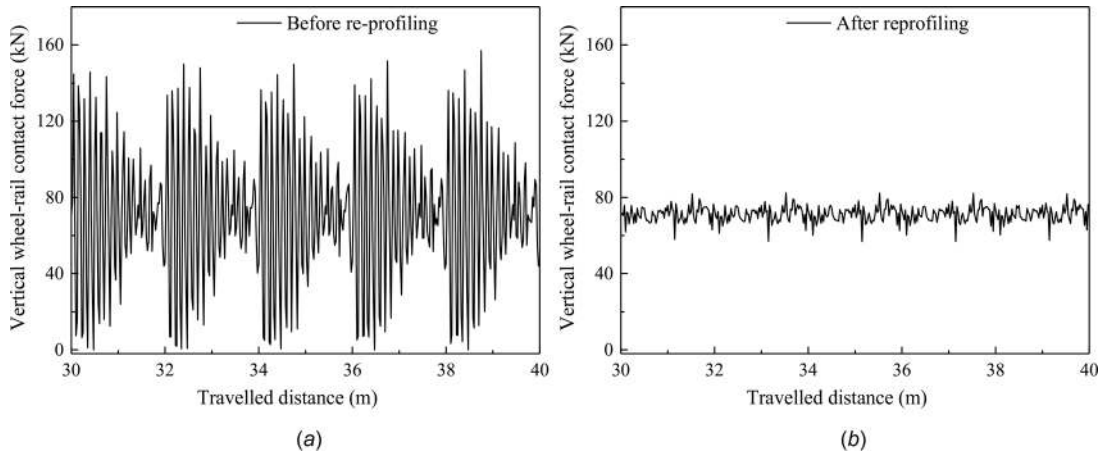

Fig. 15 The vertical wheel-rail contact forces caused by the polygonal wheel in Fig. 7(*b*) at 250 km/h. (*a*) Before and (*b*) after reprofiling [13].

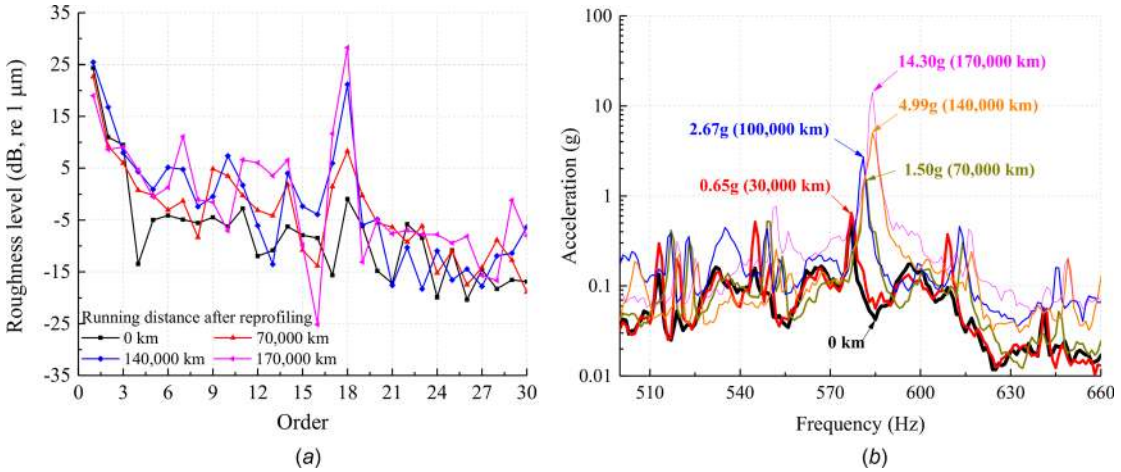

Fig. 16 Measurements conducted during 2016–2017 of a wheel on a monitored EMU running at a maximum of 300 km/h. The wheel had an initial diameter of 920 mm, but was close to its diameter limit of 830 mm during tests. (*a*) Measured roughness spectra, and (*b*) the spectra of the vertical axle box accelerations around the passing frequency of 18th-order polygonization when running on a selected section of Wuhan-Guangzhou line (close to Guangzhou) at a speed about 300 km/h.

from the measurements in Fig. 23 and photos in Fig. 24. Later, such a type of corrugation with similar wavelengths also occurred on some sections of other high-speed lines.

Besides the main line corrugation mentioned above, another type was also observed on sharp curves connecting main lines of high-speed and depots, where the passing speeds were low. This type of corrugation, as a consequence of curving behavior, mainly occurred on inner rails of the curves, and was understood to be of the well-known rutting type suggested by Grassie and Kalousek [53,56], for which the application of friction modifier was believed to be a good treatment [56,58]. Since such corrugation is not a specific problem for high-speed rails, no more information is given in this paper.

4.2.2 *Influences and Consequences*

4.2.2.1 Numerical analyses. Like wheel polygonization, rail corrugation can also excite serious high frequency wheel-rail

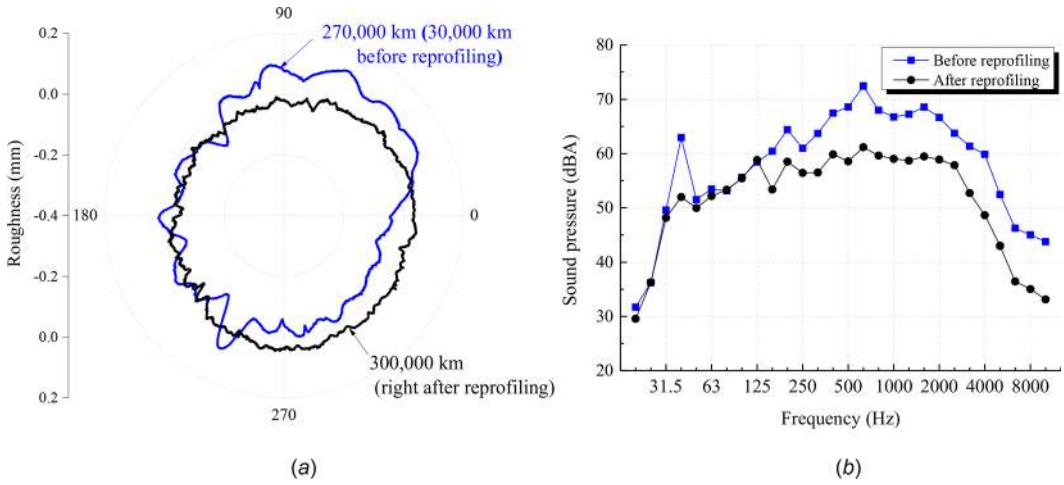

Fig. 17 Measurements of the 350 km/h EMU in Fig. 9. (*a*) Roughness spectra of a wheel before and after reprofiling, and (*b*) the corresponding noise spectra in the coach above the wheel when running at 300 km/h.

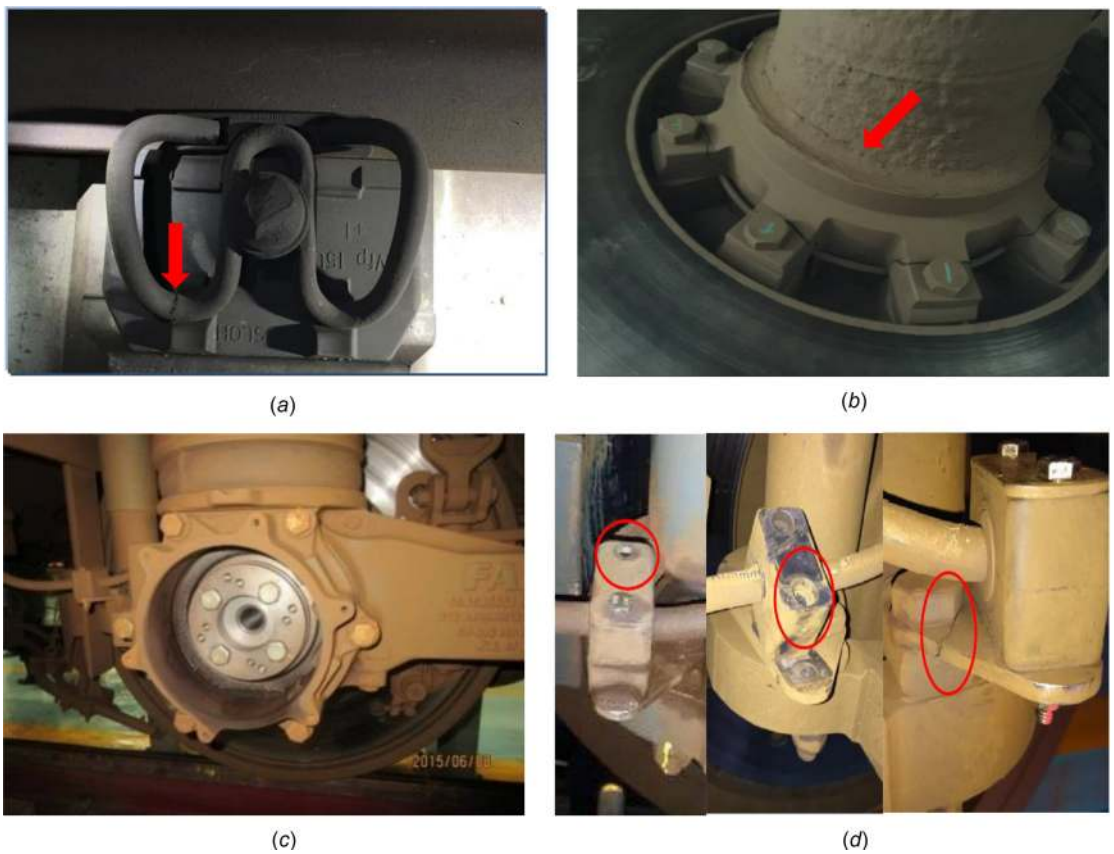

Fig. 18 Dynamic fatigue damage of vehicle and track components and accessories resulting from vibrations excited by high-order polygonization. (*a*) Fatigue of a clip, (*b*) a crack at the seat of a brake disk, (*c*) a missing axle box cover, and (*d*) missing bolts and cracks on auxiliary components of bogies.

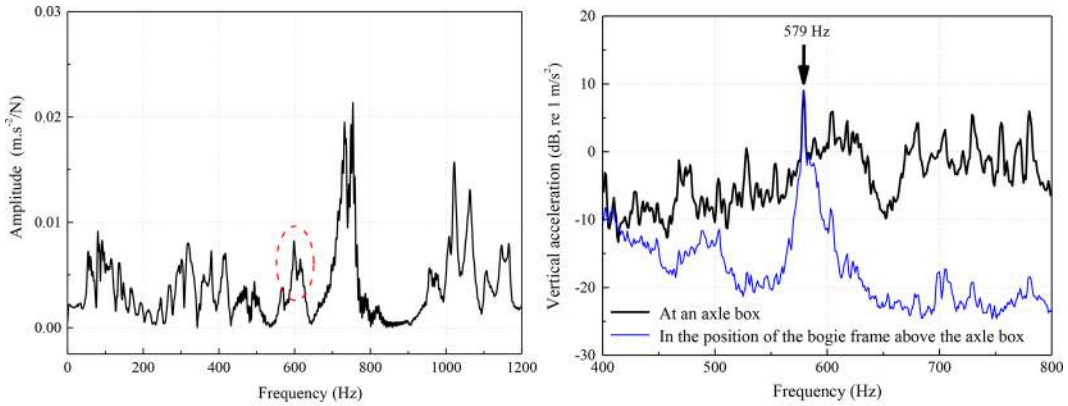

Fig. 19 Spectra of the vertical accelerations measured on the 250 km/h EMU mentioned in Sec. 4.1.2.1 [24]. (*a*) Hammer test results on a trailer measured in the position of a bogie frame right above the axle box impacted by a hammer, (*b*) running test results at 250 km/h on a motor car equipped with newly reprofiled wheels.

interactions. Figure 25 shows the vertical wheel–rail contact forces with and without corrugation calculated using the theory of vehicle–track coupled dynamics [10,11], in which the vertical irregularity of a corrugated section measured in the field and that of a typical healthy section are applied, and the corresponding speed of 300 km/h is assumed. It is seen that the vertical contact force F_N excited by the corrugation is up to 231 kN (the static load is 65 kN), much higher than that on the healthy section (105 kN). Notably, contact loss (the force vanishes) is expected at many instants.

With a transient wheel-rail rolling contact FE model [17–21], both normal and tangential rolling contact at corrugation can be analyzed in detail. Wheel-rail contact forces along three directions can be obtained together with detailed distributions of normal and tangential contact stresses (not shown in this paper). Figure 26 shows the calculated dynamic contact forces at 300 km/h in the presence of the worst corrugation observed on high-speed lines. It is seen that the vertical contact force F_N is up to 193.2 kN (the static load is 87 kN) and down to 3.02 kN (contact almost lost) in the presence of the corrugation, and the tangential force $F\tau$

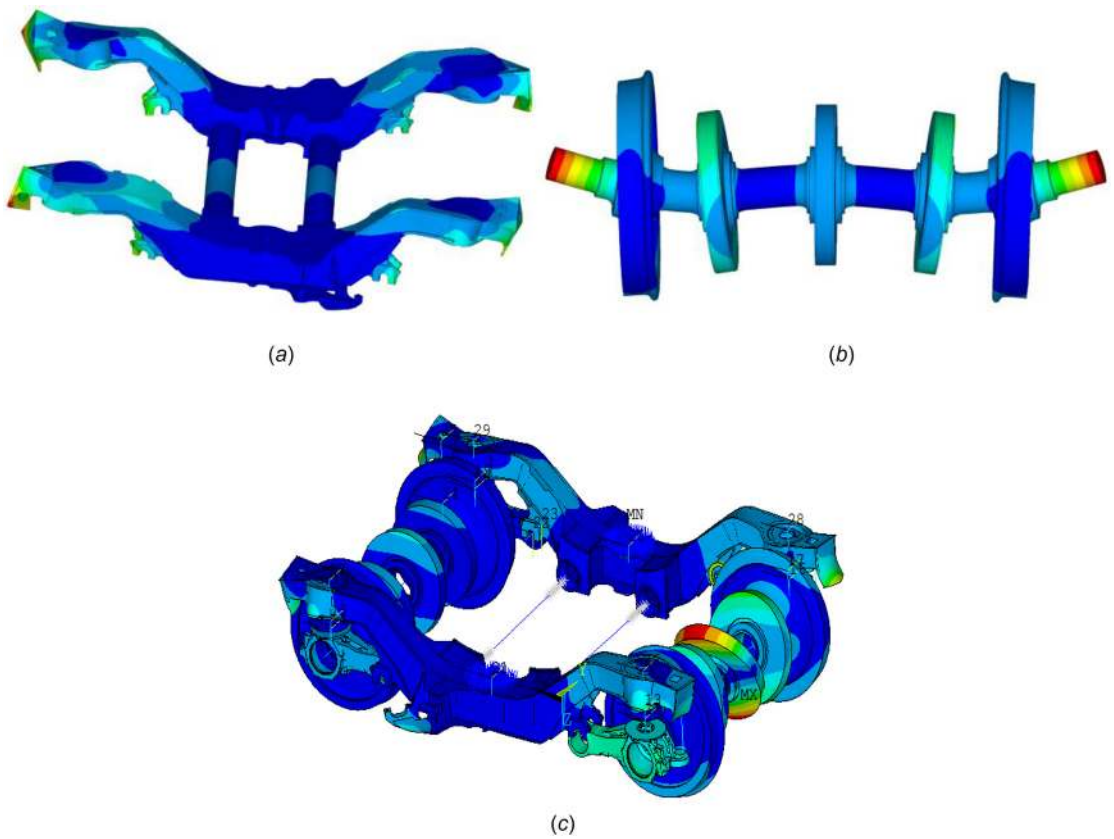

Fig. 20 Eigenmodes of a bogie and its components with frequencies around the passing frequency of 591.0 Hz calculated using the FE method for a trailer of the 250 km/h EMU mentioned in Section 4.1.2.1 [24,25]. (*a*) A bogie frame eigenmode at 590 Hz, (*b*) a wheelset eigenmode at 601 Hz, and (*c*) a bogie eigenmode at 580 Hz.

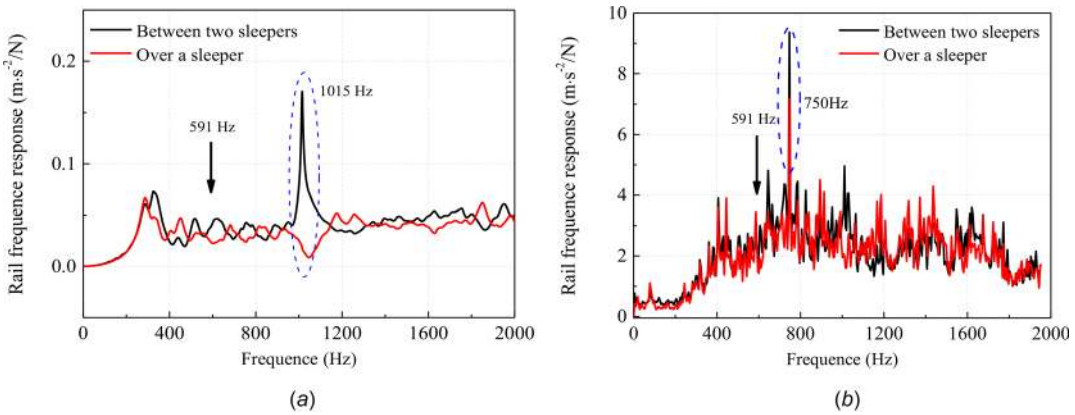

Fig. 21 Spectra of rail vertical accelerations measured on a track where the 250 km/h EMU mentioned in Sect. 4.1.2.1 ran for test [24], (*a*) Hammer test results collected at rail heads when impacted at two locations separately, (*b*) running test results collected at rail webs at about 200 km/h

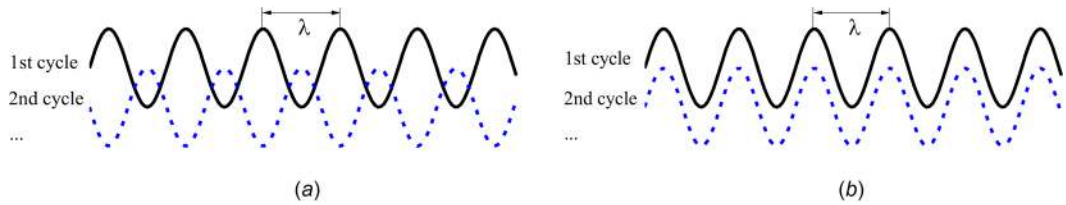

Fig. 22 Phase difference of the wear pattern in consequent cycles: (*a*) out of phase (the wavelength does not divide the circumference), (*b*) in phase (divide) leading to polygonization

coincides with fF_N at several corrugation troughs, i.e., full sliding occurs there. Note that the results in Fig. 26 are for ideal sinusoidal corrugation and include the dynamic effects of long wavelength irregularities in terms of an increased static load. This is different from the modeling approach behind the results in Fig. 25.

Comparing the results in Fig. 25 to those in Fig. 26, it is found that the dynamic forces predicted by the transient FE model are significantly lower than those predicted by the model of vehicle–track coupled dynamics. This is mainly because the continuum vibrations of wheel and rail (or the material elasticity) and detailed 3D rolling-sliding contact are considered in the transient FE approach, but not in the model of coupled dynamics [20].

4.2.2.2 Field tests. Dynamic tests were conducted in 2014 on a 250 km/h line before its opening for commercial operation, and rail roughness was also measured. Light corrugation with a wavelength of 63–80 mm was found on the rails (see Fig. 27), and resulted in a significant peak at its passing frequency (750 Hz) in the spectra of the vertical accelerations collected at rail webs (see Fig. 21(*b*)). Such results confirmed the significant vibrations excited by corrugation, corresponding well to the dynamic contact forces shown in Figs. 25 and 26. Once being excited, these vibrations could transmit upward into the vehicle system and downward into the track structure, leading to consequences such as fastening system failures, larger vibrations and noise emissions, as observed/measured on many corrugated sites.

Considering that the line was not yet open for commercial running at the time of test, it was further determined that the light corrugation shown in Fig. 27 was mainly a consequence of rail pregrinding (to remove the decarburized layer of rails). This can be seen from the grinding marks left on the rail top in Fig. 27(*b*).

4.2.3 Corrugation and Grinding Marks. Observations carried out on the high-speed line in Figs. 23 and 24 showed that corrugation only occurred on preground rails, and not on unground rails (see Fig. 28 for two examples). This suggested some significant relationships between grinding operation and the occurrence of corrugation. Further investigations into rail pregrinding and associated grinders determined that the motors of the grinding units rotated at a speed of 3400–3600 rpm (~58 r/s) during pregrinding and that, coincidently, the grinding units had an eigenmode at ~58 Hz. Thus, the eigenmode could easily be excited during operation leaving periodic grinding marks on the rail top. Under a typical grinding speed of 12–13 km/h, the wavelength of such periodic marks is 57–62 mm (see Fig. 27(*b*) for an example). A coincidence again, such a wavelength is very close to that of the *C*1 corrugation component, triggering the occurrence of additional corrugation. Such a mechanism was confirmed by the following observation: corrugation reoccurred on the line in Figs. 23 and 24 within 14 days after first trial remedy, in which the rails were reground with the same grinding strategy as the pregrinding [20].

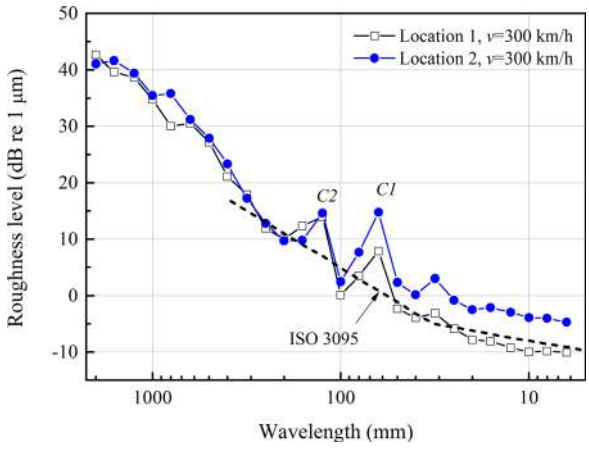

Fig. 23 Typical roughness spectra in 1/3 octave bands measured on a main high-speed line in China using a corrugation analysis trolley in 2011

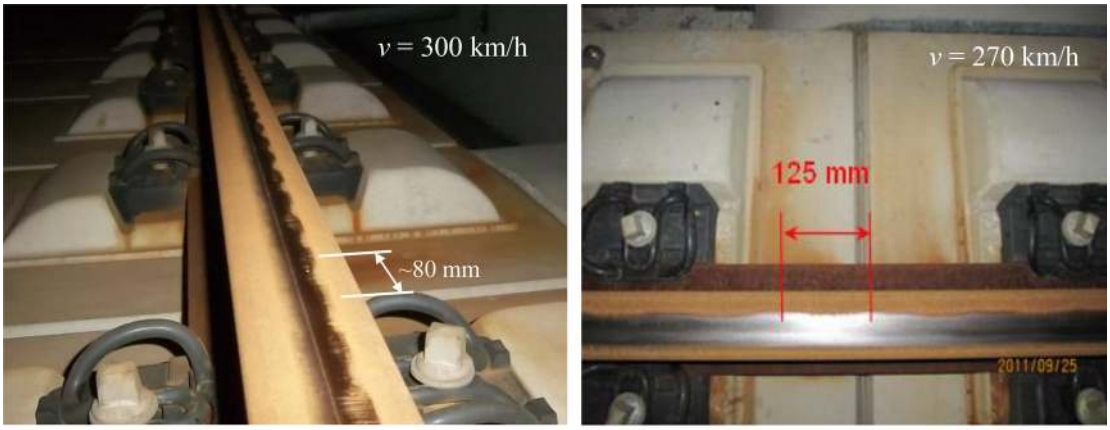

Fig. 24 Appearance of the corrugation on a Chinese high-speed line [20,23]. (*a*) *C*1 dominated corrugation, and (*b*) *C*2 dominated corrugation.

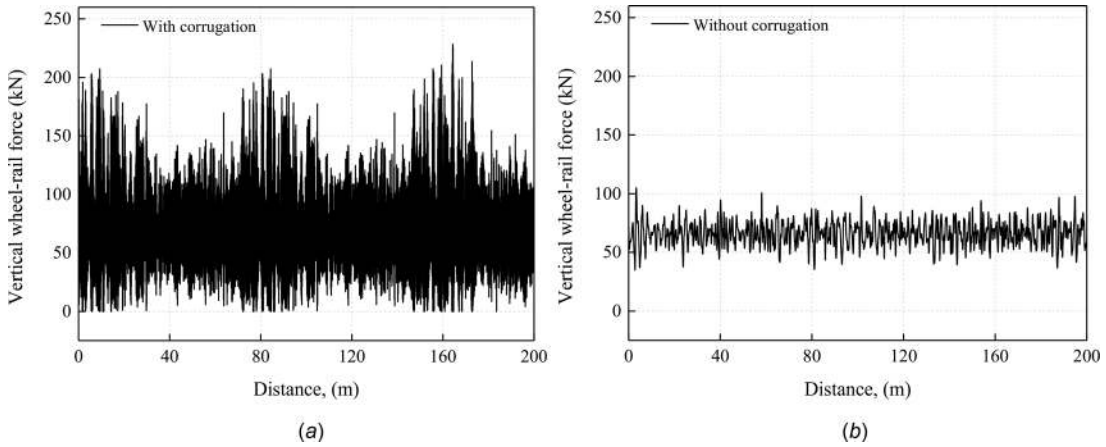

Fig. 25 The vertical wheel-rail contact forces (*a*) with and (*b*) without corrugation at 300 km/h calculated with the theory of vehicle–track coupled dynamics [12]. The wavelength of the corrugation is about 150 mm and the depth about 0.08 mm.

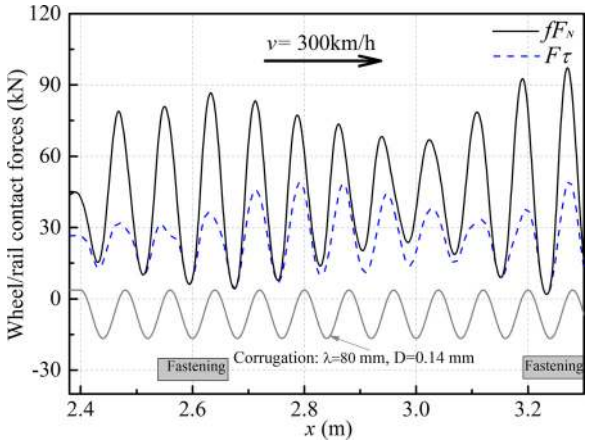

Fig. 26 Wheel-rail contact forces in the presence of corrugation with a wavelength of 80 mm and a depth of 0.14 mm calculated with a transient rolling contact FE model at 300 km/h [20]. F_N is scaled by the friction coefficient ($f = 0.5$) for comparison with F_τ.

Keeping in mind the experience of the first remedy and the above mentioned mechanism, trials were made later to modify the grinding parameters (mainly the grinding speed) in order to shift the wavelength of the grinding marks. It was later shown that a wavelength mismatch between the grinding marks and the *C*1 corrugation component could effectively prevent the occurrence of corrugation on the high-speed line. Presently, this experience has been popularized on the whole Chinese high-speed network, because of which no more significant corrugation has been reported on high-speed lines to date. Note that preventive grinding, which has been applied to high-speed rails about every 2–3 years, might also have suppressed the occurrence of corrugation to a certain extent, especially those not related to grinding marks.

5 Uneven Wear Along the Lateral Direction

Along the lateral direction, wear often concentrates on the central area of wheel profiles (close to the NRC) or on the wheel flange and rail gauge side, resulting in problems of wheel hollow wear, and wheel flange and rail side wear, respectively. Both problems have been observed in Chinese high-speed railways.

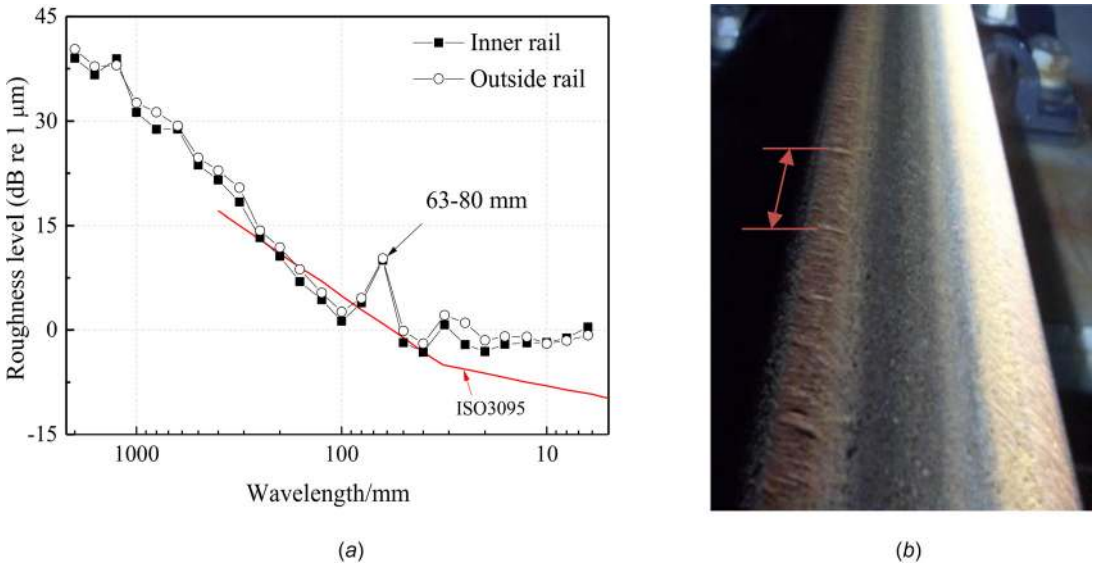

Fig. 27 Corrugation occurring on a 250 km/h line in 2014 (before its opening for commercial operation) [24]. (*a*) Roughness spectra on a curve ($R = 7000$ m) in 1/3 octave bands, and (*b*) the periodic grinding marks.

5.1 Wheel Hollow Wear

5.1.1 Observations, Measurements and Causes. The hollow wear development on wheels of EMUs running at a maximum of 350 km/h was recorded during a monitoring test conducted in south China between 2011 and 2012. From an example shown in Fig. 29(*a*), it is seen that the wear concentrated on a narrow band between −20 mm and 20 mm along the lateral direction, while the other parts remained almost unchanged. At a later stage of the test, hollow wear became visible even to the naked eye, resulting in two separated contact bands, as shown in Fig. 29(*b*) and predicted in Ref. [16].

Figure 30 shows a histogram of the hollow wear right before periodic reprofiling (i.e., the worst cases), using data from 35 high-speed bogies studied during the monitoring test. It is seen that 69.29% of the wheels exhibited hollow wear deeper than 0.2 mm and 50.71% between 0.2 mm and 0.25 mm. Thus, hollow wear was a widespread problem at that time.

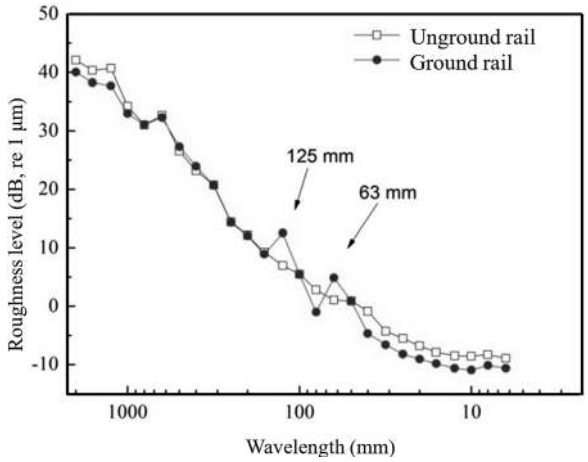

Fig. 28 Roughness spectra comparison of ground and unground rails close to a switch near which the grinders could not work [23]. An unground rail is typically 100–200 m long and the running conditions are almost the same as those on the ground rail close to it.

It is reasonable to imagine that such hollow wear is a result of narrow contact bands on the rail top, and this was indeed found to be the case, see Fig. 31. It has to be specified that such narrow contact bands on rails are required by or a consequence of the high lateral stability of the EMUs at high-speeds, i.e., the hollow wear can be considered as a side effect of the high ride comfort.

5.1.2 Consequences

5.1.2.1 Bogie hunting and anomaly alarms. Once hollow wear occurs, a wheel does not make contact with the rail at the bottom of the hollow under the assumption of rigid bodies, as shown in Fig. 32(*a*). Further, the wheel-rail contact point shifts laterally between the two edges of the hollow during running (i.e., poor steering) because of the presence of lateral track irregularities. This would be expected to lead to two contact bands on the rail top at a relatively late stage of hollow wear development, as indicated in Fig. 32(*b*) and seen from Fig. 29(*b*), as well as larger lateral vibrations of bogies and wheelsets (i.e., hunting). In addition to reduced running comfort, the increased vibration of the bogie frame might also trigger anomaly alarms for train running safety if a prescribed limit was exceeded. Actually, such alarms were the direct reason for the monitoring test conducted in 2011–2012 (Figs. 29 and 30), for which speed reduction by 10–15% had to be applied.

Figure 33 shows the spectra of lateral axle box accelerations measured above new and worn wheels during the monitoring test. Clearly, the amplitudes were much larger at frequencies of 6–9 Hz when hollow wear was present. Further calculations showed that such a frequency range corresponded to bogie hunting, confirming the above mentioned cause of the anomaly alarms.

To characterize the dynamic behavior of high-speed EMUs, a depth limit of 0.2 mm was once recommended for hollow wear based on test results and detailed simulation analyses, and found to be effective [59,60]. Recently, Cui et al. [61] proposed a dynamics approach to determine the threshold depth for wheel reprofiling with hollow wear, in which the side-wear (asymmetric wear on the two wheels of a wheelset) was also considered and the running stability, riding quality, and curving stability were all evaluated.

5.1.2.2 Rolling contact fatigue. When elasticity of wheels and rails, ignored in analyses above, is taken into account, contact may also occur at the bottom of a hollow, but with much larger

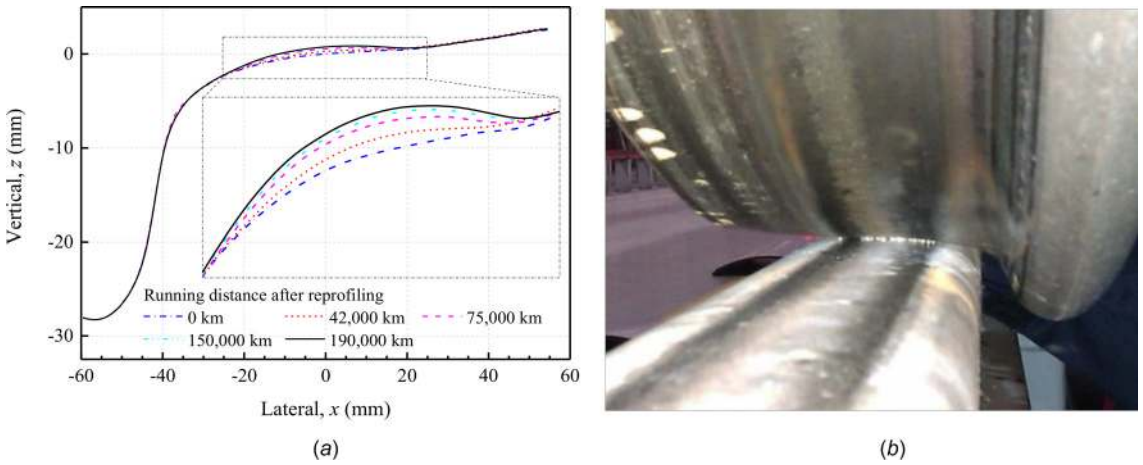

Fig. 29 Hollow wear on wheels of EMUs running in south China at a maximum of 350 km/h in 2011–2012 [42]. Laterally, $x = 0.0$ coincides with the NRC (also for similar figures later). (*a*) Profile development of a wheel and (*b*) light appearing in the contact gap between another hollow wheel and a rail.

lateral contact forces and tangential contact stresses with respect to the case without a hollow. This is mainly because of the lateral slip occurring between wheel and rail during the lateral shift of the contact patch. Such slip may accelerate the growth of the hollow, and stimulate the occurrence of RCF on the upward and downward slopes, especially when the hollow is deep. The sharper contact geometry at the edges of the hollow, i.e., the poor geometry match there, should also play a role in RCF occurrence.

Figure 34(*a*) shows a surface-initiated wheel RCF closely related to hollow wear. Such RCF occurred mainly on 250 km/h EMUs, and belonged to the class of wheel RCF on Zone 1 defined by Deuce [32]. A statistical analysis covering 47,250 km/h EMUs (conducted in the beginning of 2015) showed that significant hollow wear was found on about half of the fatigued wheels [6,7], suggesting the importance of hollow wear on the occurrence of RCF. Using the measured profiles of a monitored wheel shown in Fig. 34(*b*) and worn rail profiles measured on a line where the wheel ran, RCF was predicted to occur at the right position (in agreement with field observations) when significant hollow developed, as shown in Fig. 34(*c*). Moreover, the severest RCF was predicted to occur on the profile recorded in the second measurement, in which the deepest hollow of 0.065 mm developed, again in good agreement with the observed RCF. Numerical predictions of RCF thus confirmed the significant role that hollow wear played in RCF initiation.

It is worthwhile to mention that a hollow depth limit of 2 mm, much deeper than the above mentioned hollows of EMU wheels, was recommended from the viewpoint of surface-initiated RCF for freight wheels in Refs. [62] and [63]. The same type of depth limit for EMUs, if applicable, should be much lower due to the following reasons: (1) EMU wheels running at higher speeds are more sensitive to geometry deviations than freight wagons, and (2) the wear rate that can suppress the RCF is much smaller on the high-speed wheels due to lighter axle load and better controlled traction/braking forces.

5.2 Flange and Gauge Side Wear. Wheel flange and rail gauge side wear have been found to be very slight on the main lines of high speed rail traffic in China, as can be seen from Figs. 29(*a*) and 34(*b*). This is mainly because the minimum radii of curvature are as large as 7000 m and 3500 m on the 350 km/h and 250 km/h lines, respectively, and all lines were recently built up (see Fig. 1). Nevertheless, on tracks connecting the main lines to depots or in a yard and those close to some stations, the radius of curvature could be as low as 275 m. Severe wheel flange and rail gauge side wear have been found on such tracks (see Fig. 35 for an example). Compared to similar problems on the traditional low-speed railways, it is even more severe for high-speed railways

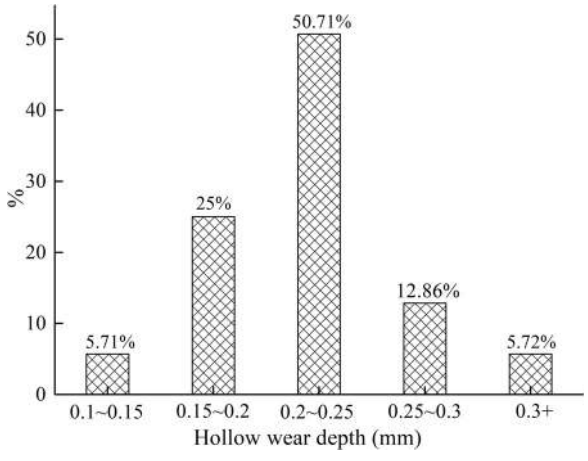

Fig. 30 A hollow wear histogram of 35 high-speed bogies (a maximum of 350 km/h) measured right before periodic reprofiling in 2011–2012 [59]

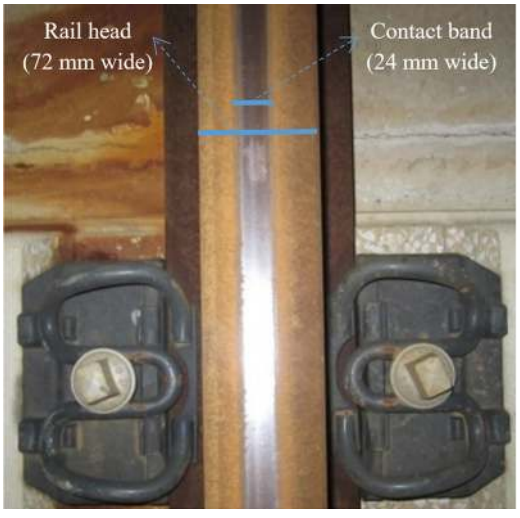

Fig. 31 A narrow contact band on the top of a high-speed rail in 2012 on a 350 km/h line

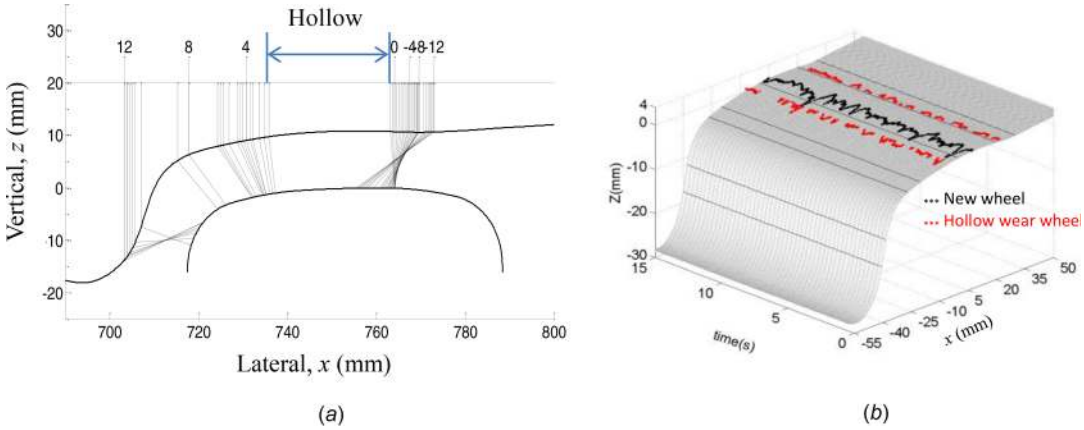

Fig. 32 Contact between a S1002CN wheel with hollow wear and a new CN60 rail. (*a*) Initial points of contact under different lateral shifts of wheelset (laterally, $x = 0.0$ coincides with the track center), and (*b*) traces of contact points on the tread calculated with a vehicle dynamics model at 350 km/h (a local coordinate system with the origin located at the rail top center is used for illustration), in which a typical irregularity of Chinese high-speed tracks was applied [60,61].

due to the relatively high primary yaw stiffness of high-speed EMUs [64].

Once flange wear occurs, relatively large material removal is required to restore the original tread profile on turning lathes, while much less removal is sufficient if a thin flange profile is applied, as indicated in Fig. 36. A series of thin flange profiles (with different flange thickness) have been designed to tackle wheels with severe flange wear, using which the service lives of high-speed wheels can be prolonged significantly. Another verified treatment against side wear is to optimize the wheel and rail profiles targeting the alleviation of the dynamic wheel–rail interaction [65]. Since this wear problem is not a specific problem related to high-speed operation and not widespread on the high-speed network, no more explanations are presented in this paper.

6 Countermeasures

Many countermeasures against the damage shown above have been introduced in the past decade. Presently, rail corrugation and wheel hollow wear have more or less been solved, as suggested above, and high-order wheel polygonization is well under control. A statistical analysis over EMUs running on a 1069 km long high-speed line showed that the number of recognized polygonal wheels decreased from 416 per month (in 2015) to below 100 after implementing a series of countermeasures (in 2016). This section summarizes the successful experience, and then presents more countermeasure proposals that have yet to be adopted.

6.1 Validated Measures

6.1.1 Against Wheel Polygonization. The first countermeasure against the occurrence of high-order polygonization of high-speed EMU wheels is to avoid long-time running at constant speeds, and to try to run on as many lines as possible. The purpose is to disturb the wear pattern along the circumference, resulting in out-of-phase wear in every cycle, so that wheel polygonization is prevented. Such a countermeasure has been validated by the monitoring test explained in Sec. 4.1.2.1.

The second countermeasure is to apply intelligent tread trimmers inspired by tread braking or cleaning. The purpose is to introduce another irregular wear to the wheel tread to offset that resulting in wheel polygonization. As illustrated in Fig. 37, the wear rate caused by a trimmer is higher at peaks of a polygonised surface and lower or nonexistence in troughs, i.e., any polygonization is effectively alleviated or even removed after sufficient operation. Trials on the Beijing-Shanghai high-speed line showed that this countermeasure was very promising, as shown in Fig. 38. More work is required to optimize the design of the tread trimmer.

6.1.2 Against Rail Corrugation. From Sec. 4.2 it is seen that the countermeasure against high-speed rail corrugation is straightforward: the grinding practice is improved to ensure that the dominant wavelengths of the grinding marks are far away from those of the corrugation. This can be achieved by either properly choosing the grinding speed or optimizing the dynamic design of grinding machines. As mentioned in Sec. 4.2.3, the effectiveness of this countermeasure has been validated in practice.

6.1.3 Against Hollow Wear. Larger equivalent conicity caused by wheel hollow is the root cause of bogie hunting and anomaly alarms. Based on detailed analyses of such anomaly alarms, a thin flange profile indicated in Fig. 39 was proposed to improve the lateral stability. The flange clearance of such a profile is about 2 mm larger, so that the rolling radius and conicity on the area close to flange root (i.e., the inner side of wheel hollow) are reduced with respect to those of the original profile, leading to a reduced equivalent conicity. In trials of the thin flange profile, it was found that the growth rate of hollow wear decreased by 50%, eliminating the anomaly alarms. Due to this success, this thin flange profile was later developed further in consideration of additional factors during field operation, and the same design idea was also applied in the development of the new high-speed wheel profile, LMb10. LMb10 has since been applied to the latest generation of Chinese CR400 series high-speed EMUs.

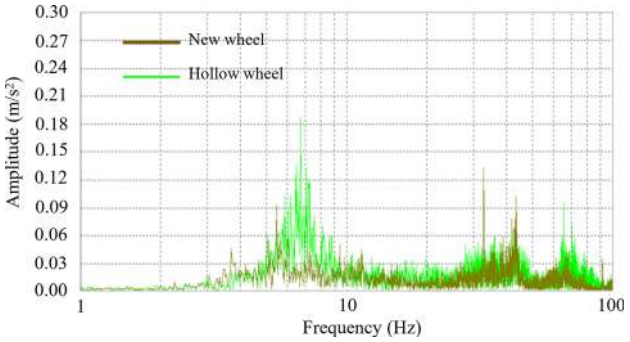

Fig. 33 Spectra of the lateral accelerations measured on axle boxes of an EMU running at 350 km/h [42]

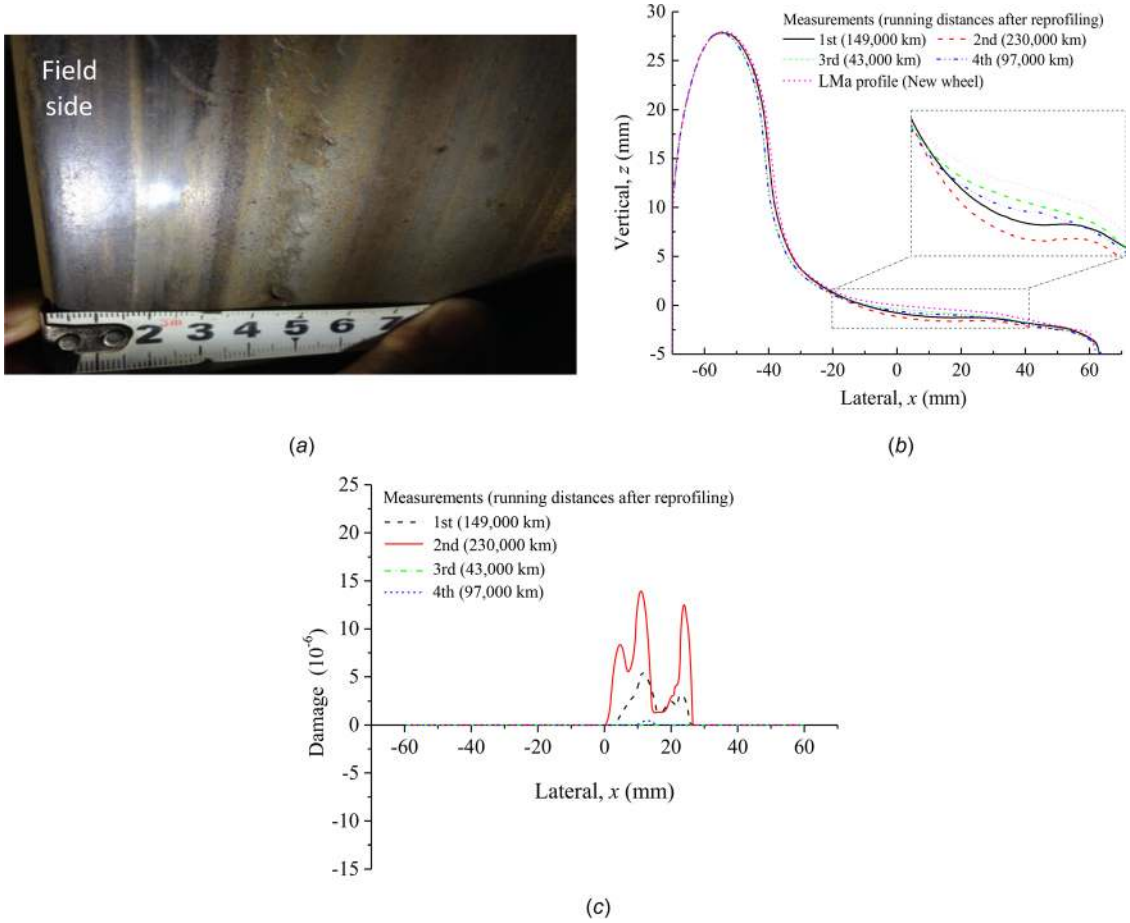

Fig. 34 Wheel RCF observed on 250 km/h EMUs and related numerical predictions [6,7]. (*a*) A typical RCF at a relatively late stage occurring on zone 1 defined by Deuce (close to the outer edge of the hollow), (*b*) measured tread geometry changes of a monitored wheel, and (*c*) predictions by $T\gamma$ model based on vehicle dynamics analyses at 250 km/h by SIMPACK in consideration of a rail profile measured on a curve of R3500 m on a 250 km/h line in south China (positive damage means RCF in the figure). Note that the wheel in (*b*) and (*c*) was reprofiled between the second and third measurements.

6.2 Measures Under Trial or Discussion

6.2.1 Against Polygonization

6.2.1.1 Better Wheel Reprofiling Strategies. It is shown above that the high-order polygonization occurring on a specific type of EMUs has an approximately constant wavelength, comes into being when the wavelength divides the wheel circumference, and decreases in order with the decrease of the wheel diameter due to wear and reprofiling. Therefore, a wheel rolling at a constant speed may be more susceptible to polygonization when its circumference or diameter reaches certain critical values. Assuming high-order polygonization corresponding to a resonance frequency of 570–580 Hz, the critical diameters calculated for different speeds using a vehicle-track coupled dynamics model [10,11] with Archard wear model embedded are shown in Fig. 40. The dark areas indicate the wheel diameter ranges in which the polygonal wear develops at high rates. It is observed that for a speed of 300 km/h the critical diameters are around 920, 874 and 830 mm, as indicated by the arrows in the figure. In order to maximize the service lives of wheels and minimize the detrimental

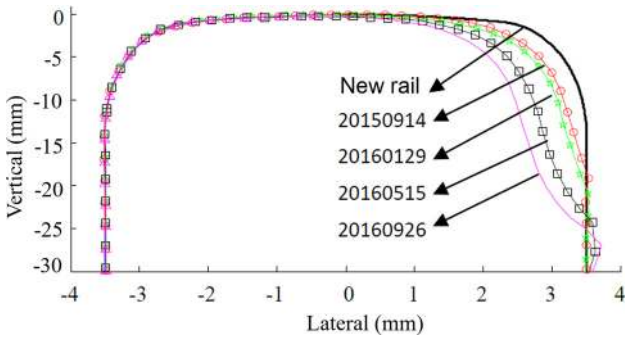

Fig. 35 The gauge side wear of the high rail on a R275 m curve in a yard

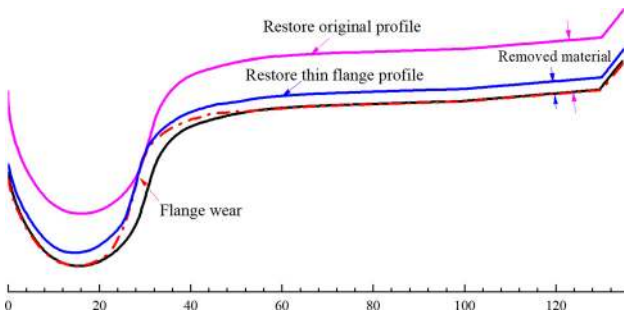

Fig. 36 A schematic diagram illustrating amounts of material removal when restoring the original wheel profile or a thin flange profile during turning

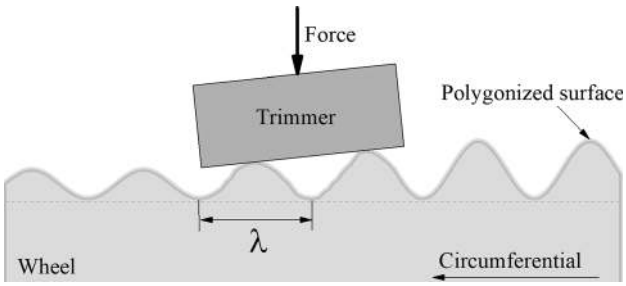

Fig. 37 A schematic diagram of the irregular wear introduced by an intelligent tread trimmer on a polygonal wheel

effects of polygonization, the reprofiling period can be shortened properly when the critical diameters are reached in practice, or large material removal may be performed to simply skip them. It is worthwhile to note that for analyses of such critical diameters, the resonance frequencies that can easily be excited under running conditions and ultimately lead to high-order polygonization should first be identified in a systematic way.

6.2.1.2 Adjustable Distance Between Drive Disks of a Turning Lathe. As shown in Fig. 10(*b*), a wheel rests on two drive disks during reprofiling on a lathe. If, coincidentally, the contact points on the two drive disks are in phase with respect to the polygonal wear, as indicated in Fig. 41(*a*), the wheel would move vertically following the polygonal wear during turning. This would lead to inefficient removal of the wheel polygonization, see Fig. 41(*b*) for an example. Practice has shown that the remaining polygonal wear, if not treated, would grow very quickly in operation, resulting in more frequent reprofiling. A simple solution to this inefficient removal, as can easily be imagined, is to introduce an extra phase shift between the two contact points, when necessary, by changing the distance L between the two drive disks.

6.2.2 Against Hollow Wear

6.2.2.1 Intelligent tread trimmer. The lateral dimension of an intelligent tread trimmer is typically wider than the wheel hollow produced by wheel-rail contact. Thus, the wear caused by a trimmer can eliminate the hollow wear to a large extent, as illustrated in Fig. 42, i.e., more material is worn away outside the hollow where the areas are relatively more proximal to the rail. The key is to find optimal operating parameters for the trimmer, with which the hollow wear can be controlled at an acceptable cost (i.e., the extra wear loss is acceptable) without significantly compromising the designed conicity.

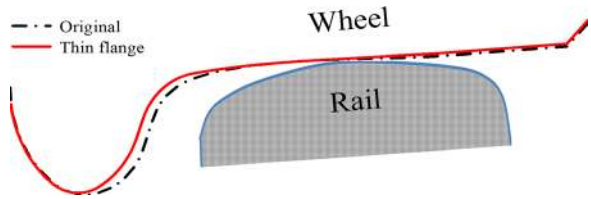

Fig. 39 Thin flange wheel profile introduced to address hollow wear

6.2.2.2 Multiple rail top profiles. It was mentioned previously that hollow wear is a consequence of a laterally concentrated wear pattern and a side effect or consequence of high running stability of EMUs. If more than one concentrated wear pattern (laterally shifted from each other) exists on the wheels running on a line, the combined wear may become relatively even, as shown in Fig. 43. An approach to such an end is to apply several different rail profiles on predivided sections of a line through rail grinding. In theory, this countermeasure is very similar to that proposed in Ref. [67], where the track gauge was varied from section to section to treat hollow wear.

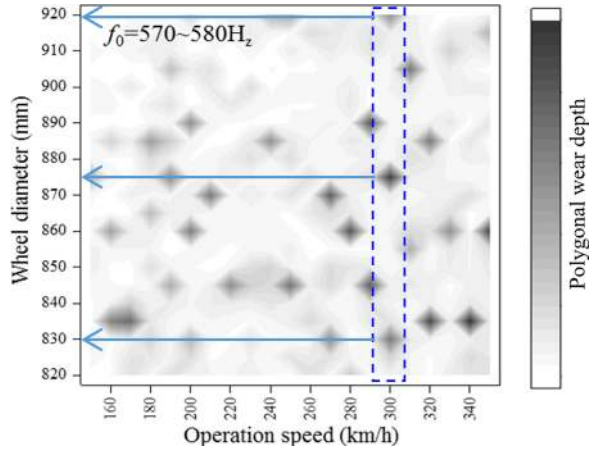

Fig. 40 Calculated critical diameters indicated in dark, at which high-order polygonization corresponding to a resonance frequency of 570–580 Hz develops at high rates [66]

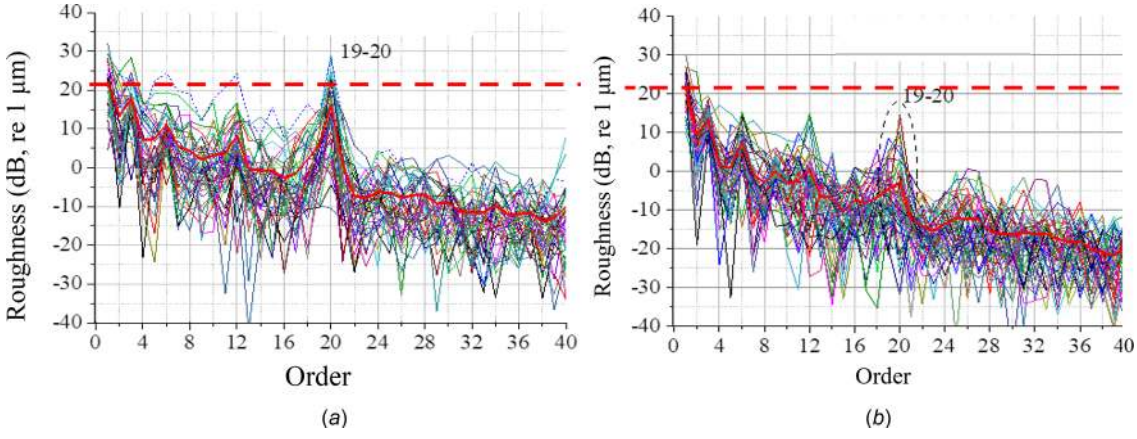

Fig. 38 Effects of intelligent tread trimmers on high-order polygonization of EMU wheels running on the Beijing-Shanghai line at a maximum of 300 km/h. Wheels after running (*a*) 177,000 km without tread trimmers and (*b*) 150,000 km with tread trimmer (unoptimized).

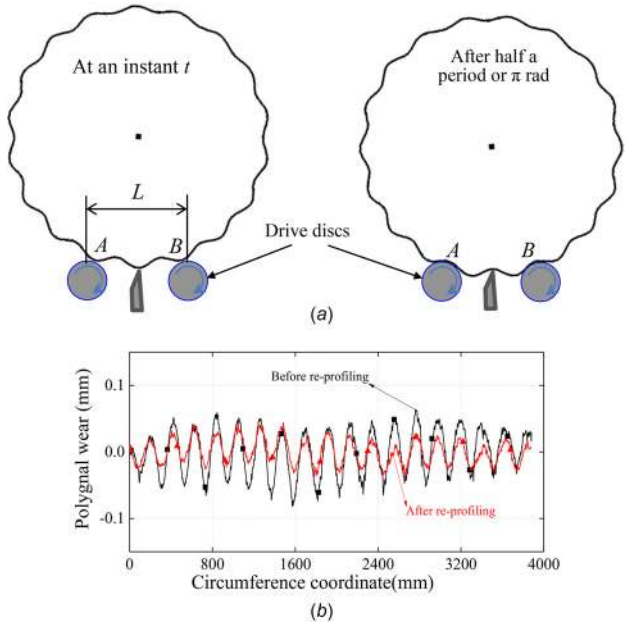

Fig. 41 Inefficient removal of high-order polygonization when the contact points on the two drive disks (*A* and *B*) are in phase: (*a*) schematic diagrams of its cause and (*b*) an example of inefficient removal

6.2.3 More Possibilities. Additional possible countermeasures against the wear problems described above, although more difficult to apply, are proposed in the following.

(1) Improved dynamic design of vehicles. By optimizing the suspension parameters or the vehicle structure, the related eigenfrequencies and eigenmodes of the vehicle-track system, e.g., those excited by the hollow wear or related to high-order polygonization, can be shifted away from the troubled frequency ranges or damped greatly, alleviating or entirely solving the problems associated with uneven wear. The keys to such a countermeasure are: (a) identify the target eigenfrequencies and eigenmodes accurately and (b) ensure that other eigenfrequencies (there are plenty of them) are not shifted into the troubled ranges.

(2) Locally hardened wheel tread. Hardened material results in lower wear rates, potentially resulting in reduced growth rates of hollow wear and high-order polygonization under the same levels of dynamic loads (although the associated problems are still there). Possible hardening techniques include laser texturing, stress peening, cold rolling, etc. Considering that the tread surface renews constantly due to wear and reprofiling during service, the hardened layer has to be deep enough to ensure its desired effects, and rehardening is probably required after larger material removal by reprofiling.

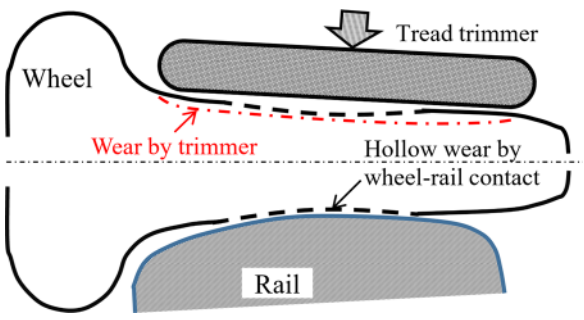

Fig. 42 Wear caused by intelligent tread trimmer to eliminate the hollow wear produced by wheel-rail contact

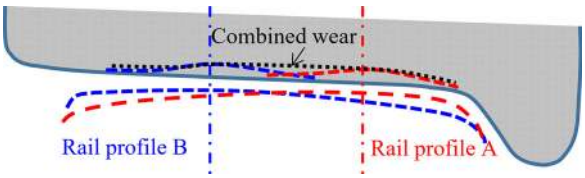

Fig. 43 A schematic diagram of the relatively even wear resulting from two hollows related to two rail profiles

(3) Better roughness or irregularity management for wheels and rails. Essentially, high-order polygonization and rail corrugation result from dynamic vibrations. If the irregularities that can excite these vibrations effectively are absent, the polygonization and corrugation would not initiate and develop easily. Such an approach has actually been confirmed by the wavelength optimization of the grinding marks mentioned above. The main issue about this countermeasure is the amount of work required for seemingly endless tracks and the large number of wheels running on the network.

(4) Timely reprofiling or grinding. Such a countermeasure is listed at last simply because it is the most straightforward and effective one for all types of damage mentioned above, but passive and very costly. A depth threshold of 0.2 mm has been recommended for reprofiling high-speed wheels with hollow wear as mentioned above, while consensus has not been reached on the thresholds for rail corrugation and wheel polygonization. Note that such a countermeasure further complicates the arrangement of preventive rail grinding and wheel reprofiling.

7 Summary and Conclusions

The understanding of and experience with uneven wear of Chinese high-speed wheel/rail systems have been summarized and explained. Two typical longitudinal wear problems, namely, wheel polygonization and rail corrugation, and two lateral wear problems, namely, wheel hollow wear and flange/gauge side wear, were described in terms of their characteristics, consequences, causes, initiation mechanisms, and treatments. The reported data and observations are mainly from first-hand field observations, monitoring tests, and dynamic measurements as well as some simulations, from which the following conclusions can be drawn.

(1) The most detrimental wheel polygonization is typically of high orders (larger than about 12) and high excitation frequencies (up to ~600 Hz) with peak-to-peak amplitude of less than 0.2 mm. Once coming into being, it leads to significant vibrations, larger contact forces and louder noise, and further accelerates damage of the related vehicle and track components such as axle boxes and rail fastenings. High-order polygonization is understood to be a consequence of a vehicle eigenmode, and tends to occur when its wavelength divides the wheel circumference, especially on wheels running at approximately constant speeds for long time during daily operation. As the wheel diameter decreases due to wear and reprofiling, the order of polygonization decreases because its wavelength stays approximately constant. Validated countermeasures include running at varying speeds and on different lines, as well as the application of intelligent tread trimmers. Low-order polygonization, something that is also present on many high-speed wheels, has not been found to be a direct cause of significant consequences due to their low passing frequencies.

(2) Rail corrugation on main lines is typically composed of two components, namely $C1$ with a wavelength of 60–80 mm and $C2$ of 120–160 mm, and its peak-to-peak amplitude is up to 0.15 mm. Periodic marks left by rail grinding, whose dominant passing frequency coincides with the vertical pinned-pinned resonance of the track, trigger the initiation and development of the corrugation. To shift the dominant wavelength of the grinding marks (i.e., to shift its passing frequency) has been validated as an effective countermeasure. The well-known rutting type of corrugation has also been observed on sharp curves of connecting lines to depots, but not a phenomenon particular to high-speed track sections.

(3) Wheel hollow wear occurring near the NRC is a consequence of narrow contact bands and high running stability of EMUs. At a depth about 0.2 mm, it becomes an urgent issue because significant hunting of bogies could be excited at 6–9 Hz by the contact patch shift between the two edges of the hollow, triggering anomaly alarms for train running safety and resulting in speed reduction. In the long term, hollow wear could also stimulate the occurrence of rolling contact fatigue. The introduction of thin flange wheel profiles targeting a lower equivalent conicity at the flange root has been proved to be an effective countermeasure. Based on this observation, the LMb10 profile has been developed for high-speed wheels.

(4) Flange/gauge side wear occurs on sharp curves connecting to depots or in a yard and sometimes on those close to stations, but not on main lines. Thus, it is not a specific problem of high-speed railways. Compared to similar problems on low-speed rails, it is even more severe due to the relatively high primary yaw stiffness of high-speed EMUs.

(5) More countermeasures under trial or demonstration include better wheel reprofiling strategies and adjustable drive disks on turning lathes to prevent the polygonization, the application of intelligent tread trimmers and multiple rail profiles to prevent hollow wear, and additional techniques such as improved dynamic design of vehicles, local hardening of wheel tread, better irregularity control for wheels and rails, and so on.

It has to be noted that most conclusions above are drawn from first-hand field data, and their direct validations, either in lab or carefully designed field tests, is still somewhat lacking. Presently, a lot of work is going on to such an end, and the related results will be published in the near future.

Funding Data

- This work was supported by the National Natural Science Foundation of China (U1734201, 11790283, 51735012, 51675444), and the Program of Introducing Talents of Discipline to Universities (111 Project) (Grant No. B16041; 10.13039/501100001809).

References

[1] National Bureau of Statistics of China, 2020, "The website of National Bureau of Statics of China," National Bureau of Statistics of China, Beijing, China, accessed Nov. 4, 2020, http://www.stats.gov.cn/tjsj/tjgb/ndtjgb/

[2] Chinese Standard, 2016, "Provisional Technical Specifications for EMUs in China," Chinese Standard, China, Chinese Standard No. TJ/CL275A-2016.

[3] National Railway Administration, 2016, "Wheel Profile for Locomotive and Car," National Railway Administration, China, Chinese Standard No. TB/T 449–2016.

[4] NSAI Standards, 2011, "Railway Applications—Wheelsets and Bogies—Wheels—Product Requirements," National Standards Authority of Ireland, Dublin, Ireland, Standard No. EN13262:2004 +A2:2011.

[5] Railway Industry Standard, 2011, "Rails for High Speed Railway," Railway Industry Standard, China, Chinese Standard No. TB/T 3276–2011.

[6] Zhao, X., Wen, Z., Liu, D., Liu, C., and Zhao, X. G., 2016, "Observations and Monitoring of the Rolling Contact Fatigue of Chinese High-Speed Wheels," 18th International Wheelset Congress, Chengdu, China, Nov. 7–10, pp. 55–59.

[7] Wang, Y., Lu, C., Zhao, X., Wen, Z., and Jin, X., 2018, "Rolling Contact Fatigue of Chinese High-Speed Wheels: Observations and Simulations," J. Mech. Eng., **54**(4), pp. 150–157 (in Chinese).

[8] Liu, F., 2016, "Tracing Research on Rail Wear in High-Speed Railway," Railway Eng., **56**(11), pp. 120–123 (in Chinese).

[9] Zhai, W., Cai, C., and Guo, S., 1996, "Coupling Model of Vertical and Lateral Vehicle/Track Interactions," Veh. Syst. Dyn., **26**(1), pp. 61–79.

[10] Zhai, W., Wang, K., and Cai, C., 2009, "Fundamentals of Vehicle-Track Coupled Dynamics," Veh. Syst. Dyn., **47**(11), pp. 1349–1376.

[11] Zhai, W., 2020, *Vehicle–Track Coupled Dynamics: Theory and Applications*, Springer Nature, Singapore.

[12] Wang, K., Liu, P., Zhai, W., Huang, C., Chen, Z., and Gao, J., 2015, "Wheel/Rail Dynamic Interaction Due to Excitation of Rail Corrugation in High-Speed Railway," Sci. China-Technol. Sci., **58**(2), pp. 226–235.

[13] Yin, Z., Wu, Y., and Han, J., 2017, "Effect of Polygonal Wear of High-Speed Rail Wheels on Vertical Force Between Wheel and Rail," J. China Railway Soc., **39**(10), pp. 26–39 (in Chinese).

[14] Chen, M., Sun, Y., Guo, Y., and Zhai, W., 2019, "Study on Effect of Wheel Polygonal Wear on High-Speed Vehicle-Track-Subgrade Vertical Interactions," Wear, **432–433**, p. 102914.

[15] Shen, Z. Y., Hedrick, J. K., and Elkins, J. A., 1983, "A Comparison of Alternative Creep Force Models for Rail Vehicle Dynamic Analysis," Veh. Syst. Dyn., **12**(1–3), pp. 79–83.

[16] Sun, Y., Guo, Y., Lv, K., Chen, M., and Zhai, W., 2019, "Effect of Hollow-Worn Wheels on the Evolution of Rail Wear," Wear, **436–437**, p. 203032.

[17] Zhao, X., Li, Z., and Dollevoet, R., 2013, "The Vertical and the Longitudinal Dynamic Responses of the Vehicle–Track System to Squat Type Short Wavelength Irregularity," Veh. Syst. Dyn., **51**(12), pp. 1918–1937.

[18] Zhao, X., Li, Z., and Dollevoet, R., 2014, "Influence of the Fastening Modeling on the Vehicle-Track Interaction at Singular Rail Surface Defects," J. Comput. Nonlinear Dyn., **9**(3), p. 031002.

[19] Zhao, X., Wen, Z., Zhu, M., and Jin, X., 2014, "A Study on High-Speed Rolling Contact Between a Wheel and a Contaminated Rail," Veh. Syst. Dyn., **52**(10), pp. 1270–1287.

[20] Zhao, X., Wen, Z., Wang, H., Jin, X., and Zhu, M., 2014, "Modeling of High-Speed Wheel-Rail Rolling Contact on a Corrugated Rail and Corrugation Development," J. Zhejiang Univ. -SCI A (Appl Phys Eng), **15**(12), pp. 946–963.

[21] Zhao, X., Zhang, P., and Wen, Z., 2019, "On the Coupling of the Vertical, Lateral and Longitudinal Wheel-Rail Interactions at High Frequencies and the Resulting Irregular Wear," Wear, **430-431**, pp. 317–326.

[22] Gu, Y., Zhao, G., Wang, H., Wen, Z., and Jin, X., 2016, "Effect of Track Vibration Characteristics on Rail Corrugation of High-Speed Railway," China Railway Sci., **37**(4), pp. 42–47 (in Chinese).

[23] Gu, Y., 2017, "Study on the Mechanism of Rail Corrugation on High-Speed Railway Unballasted Track," Ph.D. dissertation, Beijing Jiaotong University, Beijing, China (in Chinese).

[24] Wu, Y., Du, X., Zhang, H., Wen, Z., and Jin, X., 2017, "Experimental Analysis of the Mechanism of High-Order Polygonal Wear of Wheels of a High-Speed Train," J. Zhejiang Univ. - Sci A (Appl. Phys. Eng.), **18**(8), pp. 579–592.

[25] Wu, Y., Han, J., Liu, J., Liang, S., and Jin, X., 2018, "Effect of High-Speed Train Polygonal Wheels on Wheel/Rail Contact Force and Bogie Vibration," J. Mech. Eng., **54**(4), pp. 37–46 (in Chinese).

[26] Kumagai, N., Ishikawa, H., Haga, K., Kigawa, T., and Nagase, K., 1991, "Factors of Wheel Flats Occurrence and Preventive Measures," Wear, **144**(1–2), pp. 277–287.

[27] Nielsen, J., 2009, *Out-of-Round Railway Wheels," Wheel–Rail Interface Handbook*, R. Lewis and U. Olofsson, (eds.), Woodhead Publishing Limited, Cambridge, UK, pp. 245–279.

[28] Steenbergen, M. J. M. M., and Van Bezooijen, R. W., 2009, *Wheel–Rail Interface Handbook*, R. Lewis and U. Olofsson, (eds.), Woodhead Publishing Limited, Cambridge, UK, pp. 377–408.

[29] Nielsen, J., and Johansson, A., 2000, "Out-of-Round Railway Wheels—A Literature Survey," Proc. Inst. Mech. Eng., Part F: J. Rail Rapid Transit, **214**(2), pp. 79–91.

[30] Morys, B., 1999, "Enlargement of Out-of-Round Wheel Profiles on High-Speed Trains," J. Sound Vib., **227**(5), pp. 965–978.

[31] Meinke, P., and Meinke, S., 1999, "Polygonalization of Wheel Treads Caused by Static and Dynamic Unbalances," J. Sound Vibr., **227**(5), pp. 979–986.

[32] Deuce, R., 2007, *Wheel Tread Damage—an Elementary Guide*, Bombardier Transportation, Montreal, QC, Canada, p. 38.

[33] Johansson, A., and Andersson, C., 2005, "Out-of-Round Railway Wheels—A Study of Wheel Polygonalization Through Simulation of 3D Wheel-Rail Interaction and Wear," Veh. Syst. Dyn., **43**(8), pp. 539–559.

[34] Johansson, A., 2006, "Out-of-Round Railway Wheels-Assessment of Wheel Tread Irregularities in Train Traffic," J. Sound Vibr., **293**(3–5), pp. 795–806.

[35] Jin, X., Wu, L., Fang, J., Zhong, S., and Ling, L., 2012, "An Investigation Into the Mechanism of the Polygonal Wear of Metro Train Wheels and Its Effect on the Dynamic Behaviour of a Wheel/Rail System," Veh. Syst. Dyn., **50**(12), pp. 1817–1834.

[36] Li, W., Li, Y., Zhang, X., Wen, Z., Wu, L., Deng, T., and Jin, X., 2013, "Mechanism of the Polygonal Wear of Metro Train Wheels," J. Mech. Eng., **49**(18), pp. 17–22 (in Chinese).

[37] Kaper, H. P., 1988, "Wheel Corrugation on Netherlands Railways (NS): Origin and Effects of 'Polygonization' in Particular," J. Sound Vib., **120**(2), pp. 267–274.

[38] Vernersson, T., 1999, "Thermal Induced Roughness of Tread Braked Railway Wheels—Part 1: Brake Rig Experiments, and Part 2: Modeling and Field Measurements," Wear, **236**(1–2), pp. 96–116.
[39] Ahlbeck, D. R., 1987, "A Study of Dynamic Impact Load Effects Due to Railroad Wheel Profile Roughness," Tenth IAVSD Symposium, Prague, CSSR, Aug. 24–28, pp. 13–16.
[40] Ahlbeck, D. R., and Harrison, H. D., 1988, "The Effects of Wheel/Rail Impact Loading Due to Wheel Tread Runout Profiles," Nineth International Wheelset Congress, Montreal, QC, Canada, pp. 6.1.1–6.1.6.
[41] Jin, X., Wu, Y., Liang, S., and Wen, Z., 2018, "Mechanisms and Coutermeasures of Out-of-Roundness Wear on Railway Vehicle Wheels," J. Southwest Jiaotong Univ., **53**(1), pp. 1–14 (in Chinese).
[42] Cui, D., 2013, "Study on Wheel Profile Design Method for High-Speed Train," Ph.D. dissertation, Southwest Jiaotong University, Chengdu, China (in Chinese).
[43] Cui, D., Liang, S., Song, C., Deng, Y., Du, X., and Wen, Z., 2013, "Out of Round High-Speed Wheel and Its Influence on Wheel/Rail Behavior," J. Mech. Eng., **49**(18), pp. 8–16 (in Chinese).
[44] Su, J., Li, L., and Cui, D., 2017, "Study on Influence of Turning Repair Operations on Wheels With Initial Polygonal State," J. China Railway Soc., **39**(5), pp. 57–61 (in Chinese).
[45] Chen, W., Dai, H., and Luo, R., 2014, "Effect of High-Order Polygons of Wheels for High-Speed Trains on Dynamics Performance of Vehicles," Rolling Stock, **52**(12), pp. 4–8 (in Chinese).
[46] Han, G., Zhang, J., Xiao, X., Cui, D., and Jin, X., 2014, "Study on High-Speed Train Abnormal Interior Vibrations and Noise Related to Wheel Roughness," J. Mech. Eng., **50**(22), pp. 113–121 (in Chinese).
[47] Zhang, J., Han, G., Xiao, X., Wang, R., Zhao, Y., and Jin, X., 2014, "Influence of Wheel Polygonal Wear on Interior Noise of High-Speed Trains," J. Zhejiang Univ. -Sci A (Appl. Phys. Eng.), **15**(12), pp. 1002–1018.
[48] Liu, X., and Zhai, W., 2014, "Analysis of Vertical Dynamic Wheel/Rail Interaction Caused by Polygonal Wheels on High-Speed Trains," Wear, **314**(1–2), pp. 282–290.
[49] Wu, X., Rakheja, S., Qu, S., Wu, P., Zeng, J., and Ahmed, A. K. W., 2018, "Dynamic Responses of a High-Speed Railway Car Due to Wheel Polygonalisation," Veh. Syst. Dyn., **56**(12), pp. 1817–1837.
[50] Chen, G., Jin, X., Wu, P., Dai, H., and Zhou, Z., 2011, "Finite Element Study on the Generation Mechanism of Polygonal Wear of Railway Wheels," J. China Railway Soc., **33**(1), pp. 14–18 (in Chinese).
[51] Tao, G., Wen, Z., Jin, X., and Yang, X., 2020, "Polygonisation of Railway Wheels: A Critical Review," Railway Eng. Sci., **28**(4), Epub.
[52] Ahlbeck, D, R., and Daniels, L. E., 1990, "A Review of Rail Corrugation Processes Under Different Operating Modes," ASME/IEEE Joint Conference on Railroads, Chicago, IL, Apr. 17–19, pp. 13–18.
[53] Grassie, S. L., and Kalousek, J., 1993, "Rail Corrugation: Characteristics, Causes and Treatments," Proc. Inst. Mech. Eng., Part F: J. Rail Rapid Transit, **207**(1), pp. 57–68.
[54] Sato, Y., Matsumoto, A., and Knothe, K., 2002, "Review on Rail Corrugation Studies," Wear, **253**(1–2), pp. 130–139.
[55] Oostermeijer, K. H., 2008, "Review on Short Pitch Rail Corrugation Studies," Wear, **265**(9–10), pp. 1231–1237.
[56] Grassie, S. L., 2009, "Rail Corrugation: Characteristics, Causes, and Treatments," Proc. Inst. Mech. Eng., Part F: J. Rail Rapid Transit, **223**, pp. 1–16.
[57] Jin, X., Li, X., and Li, W., 2016, "Review of Rail Corrugation Progress," J. Southwest Jiaotong Univ., **51**(2), pp. 264–273 (in Chinese).
[58] Torstensson, P. T., and Schilke, M., 2013, "Rail Corrugation Growth on Small Radius Curves—Measurements and Validation of a Numerical Prediction Model," Wear, **303**(1–2), pp. 381–396.
[59] Cui, D., Wang, H., Li, L., and Jin, X., 2015, "Optimal Design of Wheel Profiles for High-Speed Trains," Proc. Inst. Mech. Eng., Part F: J. Rail Rapid Transit, **229**(3), pp. 248–261.
[60] Jin, X., Zhao, G., Liang, S., Tao, G., Cui, D., and Wen, Z., 2018, "Characteristics, Mechanisms, Influences and Counter Measurements of High-Speed Wheel/Rail Wear: Transverse Wear of Wheel Tread," J. Mech. Eng., **54**(4), pp. 3–13 (in Chinese).
[61] Cui, D., Li, L., Wang, H., Wen, Z., and Xiong, J., 2015, "High-Speed EMU Wheel Reprofiling Threshold for Complex Wear Forms From Dynamics Viewpoint," Wear, **338–339**, pp. 307–315.
[62] Fröhling, R., Ekberg, A., and Kabo, E., 2008, "The Detrimental Effects of Hollow Wear—Field Experiences and Numerical Simulations," Wear, **265**(9–10), pp. 1283–1291.
[63] Sawley, K., and Wu, H. M., 2005, "The Formation of Hollow-Worn Wheels and Their Effect on Wheel/Rail Interaction," Wear, **258**(7–8), pp. 1179–1186.
[64] Cui, D., Zhang, W., Tian, G., Li, L., Wen, Z., and Jin, X., 2016, "Designing the Key Parameters of EMU Bogie to Reduce Side Wear of Rail," Wear, **366–367**, pp. 49–59.
[65] Zhai, W., Gao, J., Liu, P., and Wang, K., 2014, "Reducing Rail Side Wear on Heavy-Haul Railway Curves Based on Wheel–Rail Dynamic Interaction," Veh. Syst. Dyn., **52**(Suppl. 1), pp. 440–454.
[66] Wu, Y., Jin, X., Cai, W., Han, J., and Xiao, X., 2020, "Key Factors of the Initiation and Development of Polygonal Wear in the Wheels of a High-Speed Train," Appl. Sci., **10**(17), p. 5880.
[67] De Cicco, T., Bracciali, A., Di Benedetto, L., and Piccioli, F., 2010, "Effetti Dell'allargamento di Scartamento Sulla Stabilita di Marcia e Sull'usura Delle Ruote Ferroviarie," XXXIX Convegno Nazionale, Maratea, Italy, Sep. 7–10, Paper No. AIAS 2010–026.